Front. Chem. Sci. Eng. 2021, 15(6): 1360–1379
https://doi.org/10.1007/s11705-021-2101-7

REVIEW ARTICLE

Scaling up of cluster beam deposition technology for catalysis application

Giuseppe Sanzone[1,2], Jinlong Yin (✉)[1], Hailin Sun[1]

1 Teer Coatings Ltd., Droitwich, Worcestershire WR9 9AS, UK
2 Quantum Solid-State Physics, Department of Physics and Astronomy, B-3001 Leuven, Belgium

© The Author(s) 2021. This article is published with open access at link.springer.com and journal.hep.com.cn

Abstract Many research works have demonstrated that the combination of atomically precise cluster deposition and theoretical calculations is able to address fundamental aspects of size-effects, cluster-support interactions, and reaction mechanisms of cluster materials. Although the wet chemistry method has been widely used to synthesize nanoparticles, the gas-phase synthesis and size-selected strategy was the only method to prepare supported metal clusters with precise numbers of atoms for a long time. However, the low throughput of the physical synthesis method has severely constrained its wider adoption for catalysis applications. In this review, we introduce the latest progress on three types of cluster source which have the most promising potential for scale-up, including sputtering gas aggregation source, pulsed microplasma cluster source, and matrix assembly cluster source. While the sputtering gas aggregation source is leading ahead with a production rate of ~20 $mg\cdot h^{-1}$, the pulsed microplasma source has the smallest physical dimensions which makes it possible to compact multiple such devices into a small volume for multiplied production rate. The matrix assembly source has the shortest development history, but already show an impressive deposition rate of ~10 $mg\cdot h^{-1}$. At the end of the review, the possible routes for further throughput scale-up are envisaged.

Keywords nanoparticle, cluster, cluster beam deposition, magnetron sputtering, heterogeneous catalysis

1 Introduction

Since the 1980s when Haruta et al. first reported that the usually inert noble metal gold exhibits good catalytic activity in nanoparticle form for carbon monoxide oxidation reaction at a temperature as low as –70 °C [1], the field of nanocatalysis has emerged and then flourished in the past few decades, and became an important branch of nanoscience and technology. In the scale of a few nanometres or below, each atom has a substantial impact on the electronic and catalytic properties of metal clusters. Hence, precise atomic control over the size and composition of clusters is critical for tuning the activity and selectivity of the clusters involved in various catalytic processes [2,3].

Over the years many approaches and techniques have been advanced to produce monodispersed small clusters or well-defined clusters with very narrow size distributions. These techniques, broadly speaking, fall into two categories: physical synthesis method and wet chemistry method. The wet chemistry approach, e.g., impregnation or precipitation, is much more widely adopted and used at industrial level to prepare the commercially available catalysts, mainly because of its ease of fabrication involved and higher nanoparticle throughput. However, wet chemical routes result in a poor control over the particle size because of the nature of their heterogeneous nucleation on the support surface [4]. The use of ligands is necessary to overcome such limitations and avoid the agglomeration of nanoparticles, but the presence of ligands on the surface of nanoparticles can block the catalytic active sites [5,6]. There are quite a few reviews published summarizing the latest progress on various aspects of this approach, for example [7], and [8].

On the contrary, the physical synthesis method can produce clusters with precise atomic control without introducing any ligands. However, it involves sophisticated vacuum equipment, which in most cases has to be operated by highly trained specialists. In addition, the throughput of the physical gas phase production is low (~1 $\mu g\cdot h^{-1}$), especially after size-selection by quadrupole mass filter or time-of-flight mass filter. Although these two

Received May 26, 2021; accepted July 22, 2021

E-mail: jinlong.yin@teercoatings.co.uk

factors have limited its wider adoption in the research community, the gas-phase synthesis and size-selected strategy was the only method to prepare supported metal clusters with precise numbers of atoms for a long time [8].

In addition to the precise atom control, the physical synthesis method, or cluster beam deposition technique, has several other potential advantages [2,9]: 1) the direct interaction between the metal cluster and the support can sometimes be tuned by the energy of the impacting particle; 2) immobilised clusters can show robust behavior against sintering at elevated temperatures and pressures, minimising the cluster agglomeration issues commonly observed during catalytic reactions; 3) the "metal-to-metal" processing produces clean and ligand-free nanoclusters; 4) mixed clusters can exhibit synergistic enhancement in catalytic activity beyond the corresponding pure clusters.

The vast majority of catalytic research of supported atomic clusters, produced by cluster beam technique, have focused on reactions under UHV (ultra-high vacuum) conditions, and more recently some endeavors have been made to investigate their catalytic properties in carefully-selected close to realistic applications, for example in electrochemistry [10–12]. Although many of these important research works have revealed the catalytic mechanism and the significant influence from cluster size and support effect on catalytic performance, the reaction conditions are still far away from realistic and industrial applications. For a model catalyst study under realistic reaction conditions, clusters should be deposited onto industrial catalyst powders and not just planar support. However, the surface area of 1 g powder (assuming a modest 10 $m^2 \cdot g^{-1}$) is 5 orders of magnitude higher than that of a typical 1 cm × 1 cm square planar substrate used for UHV or electrochemistry study. To achieve the same cluster coverage on the surfaces, the deposition time required on powder for a single sample, prepared on a state-of-the-art cluster beam deposition system, would run into months if not in years, which is not realistic or feasible [13]. The nanocluster production rate of cluster beam deposition technique must be increased by several orders of magnitude to reduce the deposition time to an acceptable level (about a few hours), which is a grand challenge.

In the past two/three decades, multiple types of cluster source have been developed in the family of cluster beam deposition technology. De Toro [14] has compared different types of cluster sources and summarized the key information in a table, as shown in Table 1, in which we added matrix assembly cluster source (MACS) in the last row to reflect the latest progress. Out of the seven type of cluster sources, the cluster production rate of thermal gas aggregation source (TGAS), laser ablation source (LAS), and pulsed-arc cluster ion source (PACIS) are significantly lower than that of the other four sources. In the case of seeded supersonic nozzle source (SSNS), although it produces a reasonably high cluster flux in excess of 10^{18} $atom \cdot s^{-1}$, the complex design needed to isolate the hot furnace from the rest of the source has restricted its usage to low-boiling point metals. Therefore, in this review, we will focus the discussions on magnetron sputtering gas aggregation source (SGAS), pulsed microplasma cluster source (PMCS), and MACS, all of which have a potential to be scaled up and produce enough amount of well-defined clusters for heterogeneous catalysis research.

Both SGAS and PMCS work in a similar way, in which the single atoms are knocked out of bulk material (called target in both techniques) via plasma sputtering process, then these single atoms would aggregate to form clusters under right conditions in gas phase. In the case of MACS, the single atoms are generated by thermal evaporation, then embedded in a cold solid argon matrix; the clusters are formed in a collision process when a beam of high energy argon ions is used to knock these atoms out of the matrix. This review paper is composed of three main sections, with each section dedicated to one particular type of cluster source. At the beginning of each section, a schematic drawing is given to show the working principle of the type of cluster source going to be discussed in that section.

Table 1 Comparison of different types of cluster sources a)

Type of source	Reported flux/($nm \cdot s^{-1}$)	Materials usable	Typical cluster size	Typical vacuum regime	Proportion of ionized particles
SSNS	~20	Low-boiling point metals	~10^0–10^3 atoms	UHV	0
TGAS	~0.05	Any material that attains 1 mbar vapor pressure at 2000 K	~10^3 atoms	UHV	0
SGAS	~100 (~1)	Virtually any solid (using RF or HiPIMS for insulators)	1–60 nm	HV	Up to 50%
LAS	~0.1	Virtually any solid	~10^0–10^2 atoms	UHV	≈10%
PACIS	~1	Virtually any solid	1–10 nm	HV	≈10%
PMCS	1–30	Conductive solids	~10^1–10^4 atoms	UHV	≈10%
MACS	10 $mg \cdot h^{-1}$	Any metal can be vaporised	~10^0–10^3 atoms	HV	0

a) Reprinted with permission from ref. [14], copyright 2017, John Wiley and Sons. RF: radio frequency; HiPIMS: high-power impulse magnetron sputtering.

2 Sputtering gas aggregation source

2.1 Magnetron sputtering process

The sputtering process is induced by the energetic ion bombardment onto the cathode surface (the target), which is made of the material desired to form the atomic vapor, via multiple momentum transfers in a cascade process which results in knocking-off the target atoms from the surface to the gas phase. The ratio between the number of ions bombarding the target surface and the target atoms ejected is referred to as the sputtering yield. The sputtering yield depends on the energy of the impinging ions, target material and ion species as well as geometrical factors such as angle of incidence [15–22].

Figure 1 shows the working principle of the magnetron sputtering process. With the employment of a magnetic field underneath the target, the electrons in the plasma are confined in a small region close to the target surface (Fig. 1(a)), enhancing the gas ionization and therefore increasing the plasma density, and extending the range of pressure under which the sputtering process can be sustained [23–25]. When magnets are involved, the process is more commonly referred to as magnetron sputtering [26], and the target and magnets assembly is called magnetron. As the plasma is more localized in the region of electron confinement, the sputtering process will also be confined in a smaller portion of the target surface accordingly [27,28]. As erosion goes on, a racetrack becomes more and more visible where the target has been eroded (Fig. 1(b)).

Magnetron sputtering has become a widely spread technique, both industrially and academically, to deposit thin films. Because of the nature of the process involving an electrical potential applied to a target and gas at low pressure, it has a huge versatility in terms of materials that can be ablated. Although only electrically conductive materials can be sputtered when using direct current (DC) power supply, it is possible to run a sputtering process even in the case of insulators and dielectric materials by using a RF power supply [29]. Furthermore, with the introduction of reactive gas in the process, the gas species can combine with the sputtered species to form compounds, allowing deposition of oxides, nitrides, carbides, and even more complex materials. The composition can be tuned by changing the reactive gas flow rate, power applied to the magnetron or gas pressure used during the process [14,30].

2.2 Magnetron sputtering cluster source

Magnetron sputtering is characterized by a high degree of ionization of the sputtered material [14], which, together with the afore-mentioned advantages, makes the technique highly versatile for cluster synthesis in the gas phase. It was in the early 1990s that Haberland and coworkers employed the magnetron sputtering as a vaporization technique for a cluster source [31,32]. Figure 2 shows a schematic cross section of the magnetron sputtering cluster source, as developed by Haberland et al. The sputtering chamber (also called condensation chamber, as the sputtered atoms also condense to form clusters within the same chamber), where the sputtering process occurs, is contained in a bigger chamber, which has the pumping system attached to. The gas is injected inside the sputtering chamber, and its flow rate controlled by mass flow meters. The sputtering chamber is linked to the bigger chamber via a small orifice, i.e., the nozzle (typically with a size in the range of ~1–10 mm), which works as a leaking gas barrier to separate two pressure zones. A higher pressure builds up inside the sputtering chamber typically in the range of ~10–100 Pa, while the pressure outside is much lower at 0.01–0.1 Pa, where a long mean free path is required to have a collision-less cluster beam. A higher pressure inside the sputtering chamber helps the sputtered atomic vapor to condense and form clusters. For this reason, the sputtering chamber is often referred to as condensation or aggregation

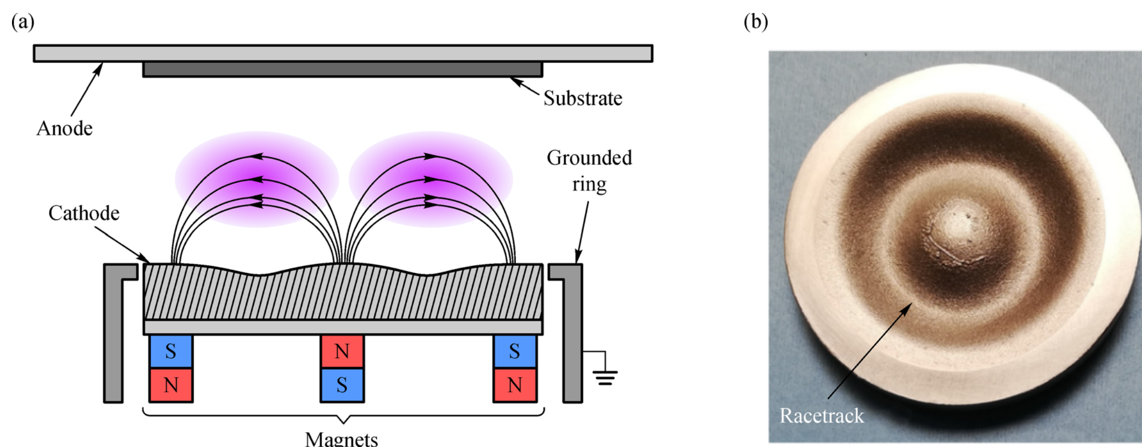

Fig. 1 (a) Cross section schematics of a planar magnetron. Reprinted with permission from ref. [27], copyright 2020, Elsevier. (b) A racetrack developed on a 2-inch circular aluminum target, showing the target erosion in a magnetron sputtering process.

chamber or even cluster source section. Because of the pressure difference between the two chambers, the gas (and the transported clusters) experiences a supersonic expansion. A skimmer placed downstream helps remove the excess carrier gas and only the central part of the beam, rich in clusters, travels in the form of a collision-less cluster beam into the next chamber for deposition. If needed, another chamber can be added in-between when, for example, mass filtering or ion optics is necessary.

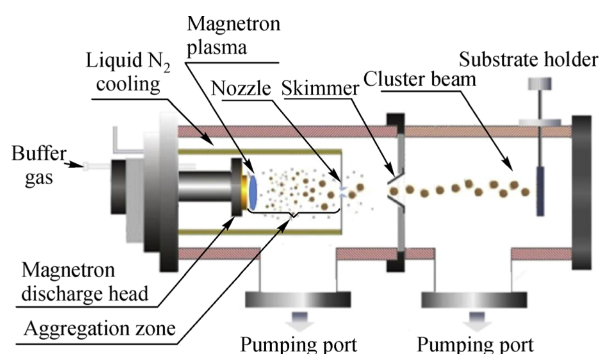

Fig. 2 Schematic drawing of the cross section of a magnetron sputtering cluster source. Reprinted with permission from ref. [33], copyright 2020, Elsevier.

There are several parameters that influence the cluster size, flux, and ionization rate. The following is a list of the easy-to-access parameters affecting cluster growth, throughput, and charge state: 1) Aggregation length, i.e., the distance between the sputtering target and the nozzle. The greater this distance, the longer the cluster residence time inside the aggregation chamber. This means they have more chances to collide with the surrounding sputtered material, therefore growing larger [34,35]. 2) Sputtering power, it affects the amount of sputtered atoms, the temperature and the ionization of the gas, which in turn influences the cluster growth and charging state [33,34,36–38]. 3) Reactive gas, enhancing the formation of dimers, which act as seeds in the cluster growth process [37,39,40]. 4) Inert gas composition and flow rate, they influence not only the pressure but also the ejected target atom thermalization efficiency as well as plasma properties which eventually affects the particle charge state [36]. 5) Temperature of the chamber wall, a lower temperature increases the thermalization efficiency thus promoting the cluster nucleation and growth rates [41,42]. If working at a lower temperature is required, the aggregation chamber wall can be equipped with a double skin structure to allow circulation of water or another coolant (e.g., liquid nitrogen).

2.3 Scaling up of magnetron sputtering cluster source

Owing to the flexibility, reliability and reproducibility offered by a magnetron sputtering cluster source, it has become the most used type of cluster source, and the only type of cluster source that is available on the market offered by a few instrument companies. Many research groups also built different variations of the magnetron sputtering cluster source for their own research interest and purpose. However, the cluster throughput has been largely unchanged since its invention in the early 1990s. The typical beam current, a measure of the cluster flux, is around 100 pA, which can be roughly translated into a deposition rate of ~1 $\mu g \cdot h^{-1}$ (assuming cluster Au_{1000} being deposited) as all the metallic clusters are singly charged. This flux is more than adequate for fundamental surface science study or catalysis mechanism study under UHV conditions. However, the throughput must be improved by several order of magnitude to meet the requirement of catalysis research under realistic condition, which has been identified as one of the most important applications of well-defined nanoclusters.

To scale up the magnetron sputtering cluster source, several approaches have been taken by different research groups, with an aim to further extend its capabilities and performance. Here we select three key approaches and describe them in detail: 1) multiple ion cluster source (MICS), where different cathodes are employed at the same time, but independently controlled; 2) HiPIMS, which provides high power density in short power pulses to the target; 3) gas dynamics modification, through which to optimise the cluster transport for a higher cluster throughput.

2.3.1 Multiple ion cluster source

The MICS is a patented design [43], in which the single magnetron in an ordinary magnetron sputtering cluster source has been replaced with three independent magnetrons. Each magnetron is independently provided with cooling water, gas inlet, power supply, and linear drive. The linear drive on each magnetron is used to adjust its relative distance with the other two and with the nozzle. As the position, the gas flow rate and the power applied to the target are all controlled individually for each magnetron, the multi-magnetron approach offers new possibilities for cluster synthesis. In particular, it has been demonstrated that it is possible to control over the cluster shape similar to ordinary magnetron sputter cluster sources [44–47]. By tuning the relative distance of the magnetrons with each other and with the nozzle, it is possible to prepare alloy clusters [48], with different elements mixed uniformly in the cluster, or core-shell clusters [49], where a core of a pure element is coated by a pure shell of another element, or even core-shell-shell structures [49] (Fig. 3).

If all the three magnetrons are in-plane, i.e., with the same aggregation length, the atoms ejected by the three

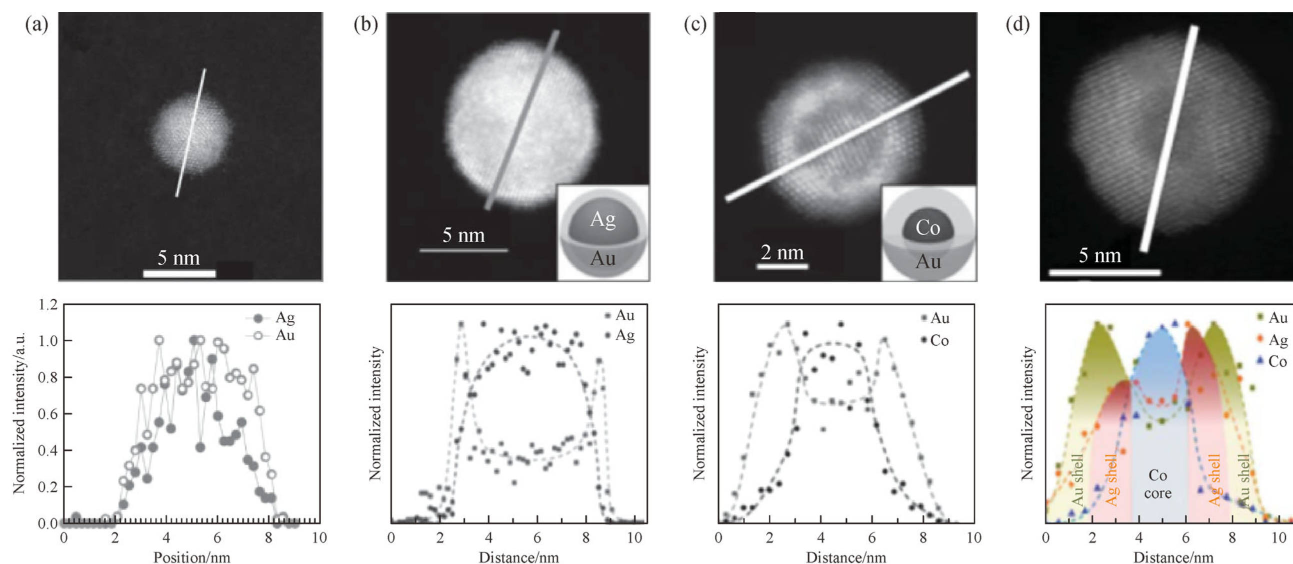

Fig. 3 (a) High resolution transmission electron microscope image of a Ag-Au alloy nanoparticle (NP) and energy dispersive spectrometer (EDS) line scan performed at the Ag and Au along the line depicted. Reprinted with permission from ref. [48], copyright 2012, American Chemical Society. (b), (c) and (d) Cs-corrected scanning transmission electron microscope (STEM) representative image of, respectively, a Ag-Au core-shell NP, Co-Au core-shell NP and a Co-Ag-Au core-shell-shell NP and EDS line scan performed at the Co, Ag, and Au, along the lines depicted. Reprinted with permission from ref. [49], copyright 2014, the Royal Society of Chemistry.

targets will nucleate and grow intermixing with each other, forming alloy clusters as they occupy the same spatial region. The composition can be tuned by changing the power and/or gas flow rate differently for the three magnetrons. If a magnetron is placed at a longer aggregation length with respect to the other two, the atoms ejected by its target will start forming clusters not contaminated by the other two elements, which are further away downstream in the aggregation chamber. As these clusters are transported to the region where the other two magnetron sputtering processes occur, they will be surrounded by the atomic vapor of the other two elements, which will attach to the surface of the preformed clusters, coating them and eventually forming a film. Analogously, if the three magnetrons have all different aggregation lengths, core-shell-shell structures might be obtainable.

Despite showing many advantages, one limitation is the introduction of new complexities, such as the relative position of the magnetrons, and new parameters which need to be considered when running a process, such as the total gas flow rate, which is the sum of the three gas flow rate contributions coming from the three magnetrons.

The reported cluster flux of MICS is 20 $NP\cdot\mu m^{-2}\cdot s^{-1}$ at a sputtering power of 8 W [50], which is equivalent to ~300 $\mu g\cdot h^{-1}$. This seems to be a dramatic increase, comparing to a typical value of 1 $\mu g\cdot h^{-1}$; but this flux was measured before mass selection, so the actual improvement might be moderate. The advantage of MICS is the capability to produce bi-metallic or tri-metallic nanoclusters, which are hugely interesting for catalysis research.

2.3.2 High-power impulse magnetron sputtering

Carrying an electric charge is important for a cluster especially when the manipulation of the cluster beam, such as focusing and bending or mass filtering, is needed. The most straightforward way to increase the amount of charged particles, or more in general the overall amount of clusters, is to increase the power applied to the magnetron. However, this comes with the physical limitations imposed by the application of a high DC power, as the risks of overheating and eventually melting the target increase.

An alternative solution is to modulate the power applied from a continuous to a pulsed regime. A pulse is characterized by a high peak power density, providing a much higher ionization rate of the sputtered species while not exceeding the time-averaged power limit. The parameters to consider in a pulsed power operation mode are the peak power intensity, pulse duration and frequency of the pulses. As a general guideline, the time-integrated power density should not exceed 0.05 $kW\cdot cm^{-2}$ to avoid any target damage [51].

The HiPIMS is established when the peak power is greater than ~0.5 $kW\cdot cm^{-2}$, however this is not a well-defined limit. The technique is characterized by a sputtering process where a large fraction of the sputtered atoms is ionized [51–53].

Pulsed DC has been employed in Haberland-type magnetron sputtering cluster sources by several research groups. Polonskyi et al. [54] demonstrated how the deposition rate of TiO_x clusters can be increased by a

factor of 20 if DC magnetron sputtering is replaced by pulsed DC (Fig. 4). Zhang et al. [55] studied the growth mechanisms of Ag clusters generated by HiPIMS. They showed how Ag cluster size can increase with the peak power and the pulse frequency. In the latter case, cluster bunches generated by each pulse can overlap, leading to an overall higher ion current, up to ~250 nA (Fig. 5). Straňák et al. [56] synthesized Cu clusters using HiPIMS, showing control over the cluster size for pressure under 30 Pa and highlighting one of the issues faced with this technique: cluster flux is suppressed at higher pressure.

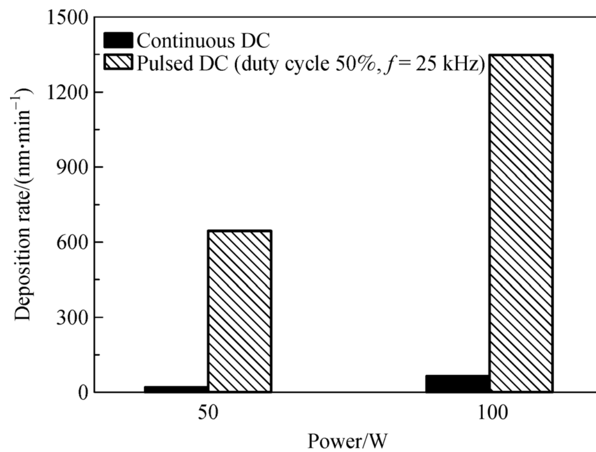

Fig. 4 TiO_x cluster deposition rate generated by continuous DC (solid fill) and pulsed DC (textured fill) under two different power applied (50 and 100 W). Reprinted with permission from ref. [54], copyright 2013, AIP Publishing.

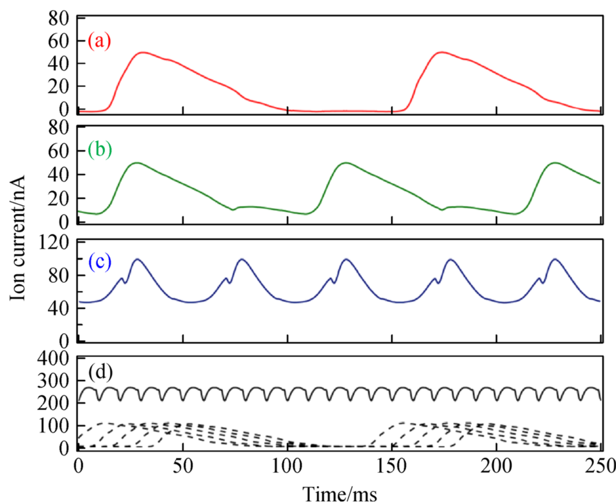

Fig. 5 Time-resolved ion current measurements for different pulse frequencies: (a) 7, (b) 10, (c) 20, and (d) 100 Hz (The dashed lines in (d) show the deconvolution in five traces as shown in (a)). Reprinted with permission from ref. [55], copyright 2013, American Chemical Society.

To overcome the limitation of operating at a low pressure, Pilch and coworkers implemented HiPIMS in a hollow cathode sputtering device [57,58], which shows not only a more stable sputtering at higher pressures but also an increase of the amount of ionized sputtered atoms [59]. By implementing such modifications, they raised the deposition rate for Cu clusters from 3 to 470 $nm \cdot s^{-1}$.

The authors also proposed a model to explain such increment in the deposition rate, as shown in Fig. 6. The initial growth of a cluster by nucleation, cluster formation, and aggregation, up to a size of about 10 nm in diameter, is shown in Fig. 6(a), and further growth under conditions, such that electric attraction toward the cluster has a large effect on the ion collection rate, is illustrated in Fig. 6(b). The advantage of increasing the amount of ionized sputtered atoms in the gas phase is to promote cluster growth processes. In early growth stages, due to the unbalanced current of ions and electrons to clusters, particles can be found in a charged state, mainly negative for particles with a diameter ~10 nm. This results in cluster repulsion, hindering their growth by cluster agglomeration (zone I in Fig. 6(c)), and cluster growth would further proceed only by attachment of atoms or ions (zone II in Fig. 6(c)). The collision cross section is larger for opposite charged particles. Therefore, charged clusters will have a higher ion collection rate, establishing the so-called orbit motion limited (OML) collection of ions (Fig. 6(b)). This means a higher growth rate, and since the concentration of ions is much higher than in standard magnetron sputtering, the result is an overall increment of the cluster mass flux. An anode ring is also placed at a variable distance from the hollow cathode. The space between the anode and the cathode has a high electron temperature T_e, which enhances the OML collection of ions (Fig. 6(d)). Figure 7 shows deposition of clusters for three different distances between the anode ring and the cathode. In general, the larger the distance, the longer the clusters grow by OML collection of ions and the bigger they become.

2.3.3 Gas dynamics influence

After a cluster is formed inside the condensation chamber, it either diffuses to the chamber wall and lands there, or may diffuse to the center of the chamber, follow the drifting carrier gas, and leave the chamber through the exit nozzle. A better understanding of how a cluster behaves aerodynamically, would guide the design of a more efficient cluster source which should minimise the possibility of clusters landing at chamber wall hence increase the portion of clusters forming a beam and being deposited on a substrate. Assisted by aerodynamic simulation, Sanzone et al. investigated how gas inlet position and chamber shape configuration influence the cluster flux, and disclosed some of the mechanisms related to the cluster transportation in a confined condensation chamber [35].

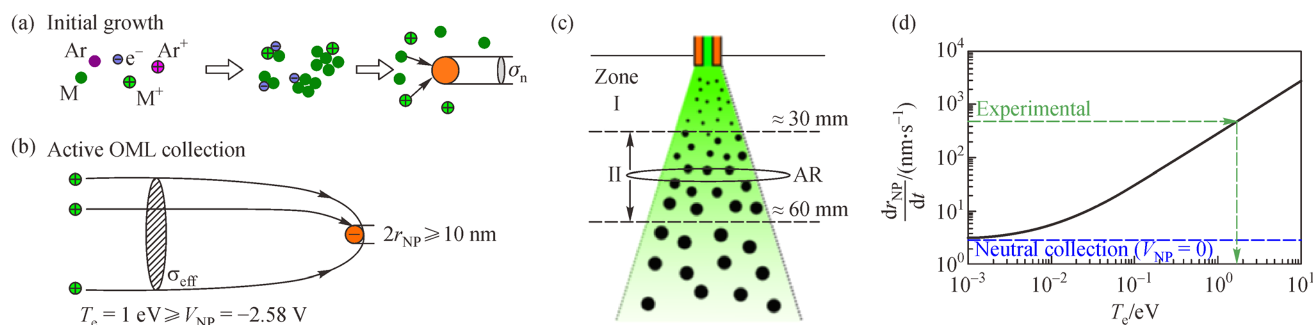

Fig. 6 (a) Sketch of the early-stage cluster growth, occurring in Zone I in (c); (b) sketch of the OML collection of ions process, showing a much larger cross section compared to the neutral case; (c) schematic drawing of the regions corresponding to different stages of cluster growth. A movable anode ring is installed to tune the size of the second cluster growth region; (d) cluster growth rate for OML collection of ions as a function of the electron temperature T_e. The neutral collection rate (blue dashed line) is 2.8 nm·s^{-1}, while for the experimental observed growth rate by OML collection of 470 nm·s^{-1}, T_e needs to be 1.7 eV. Reprinted with permission from ref. [58], copyright 2013, AIP Publishing.

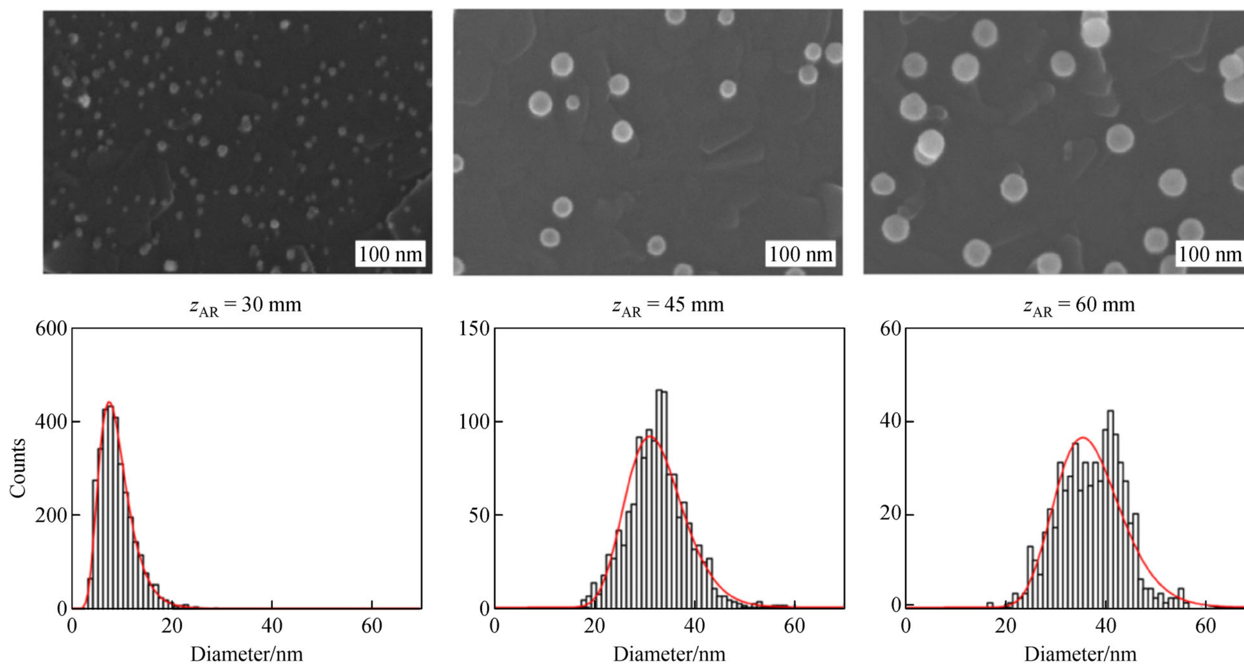

Fig. 7 Scanning electron microscopy images and calculated size distribution for anode ring position at 30, 45, and 60 mm from the hollow cathode. Reprinted with permission from ref. [58], copyright 2013, AIP Publishing.

It was found experimentally that the cluster flux is more than 20 times higher when the carrier gas inlet is located inside the magnetron sputtering source, comparing to when it's located at the rear of the chamber, even though almost 4 times higher sputtering power was used for the latter case (31 W *vs.* 8 W). Overall, the former case is almost 80 times more efficient in terms of cluster production. To investigate the potential causes of this significant difference in cluster flux, gas flow dynamics simulations were carried out.

The simulation results (Fig. 8) have shown that if the gas is provided through the magnetron source itself, the sputtered single atoms are distributed within a much narrower space along the central axis of the condensation chamber, which results in a local high number density of single atoms, hence enhancing the cluster formation and growth. For the other inlet configuration, where the gas is introduced from the rear of the chamber, the sputtered atoms are distributed more broadly in the chamber, which can be translated into lower probability for the three-body collisions to happen (Fig. 8(c)) due to lower number density of single atoms. The three-body collision is the critical step for cluster nucleation process. To design a

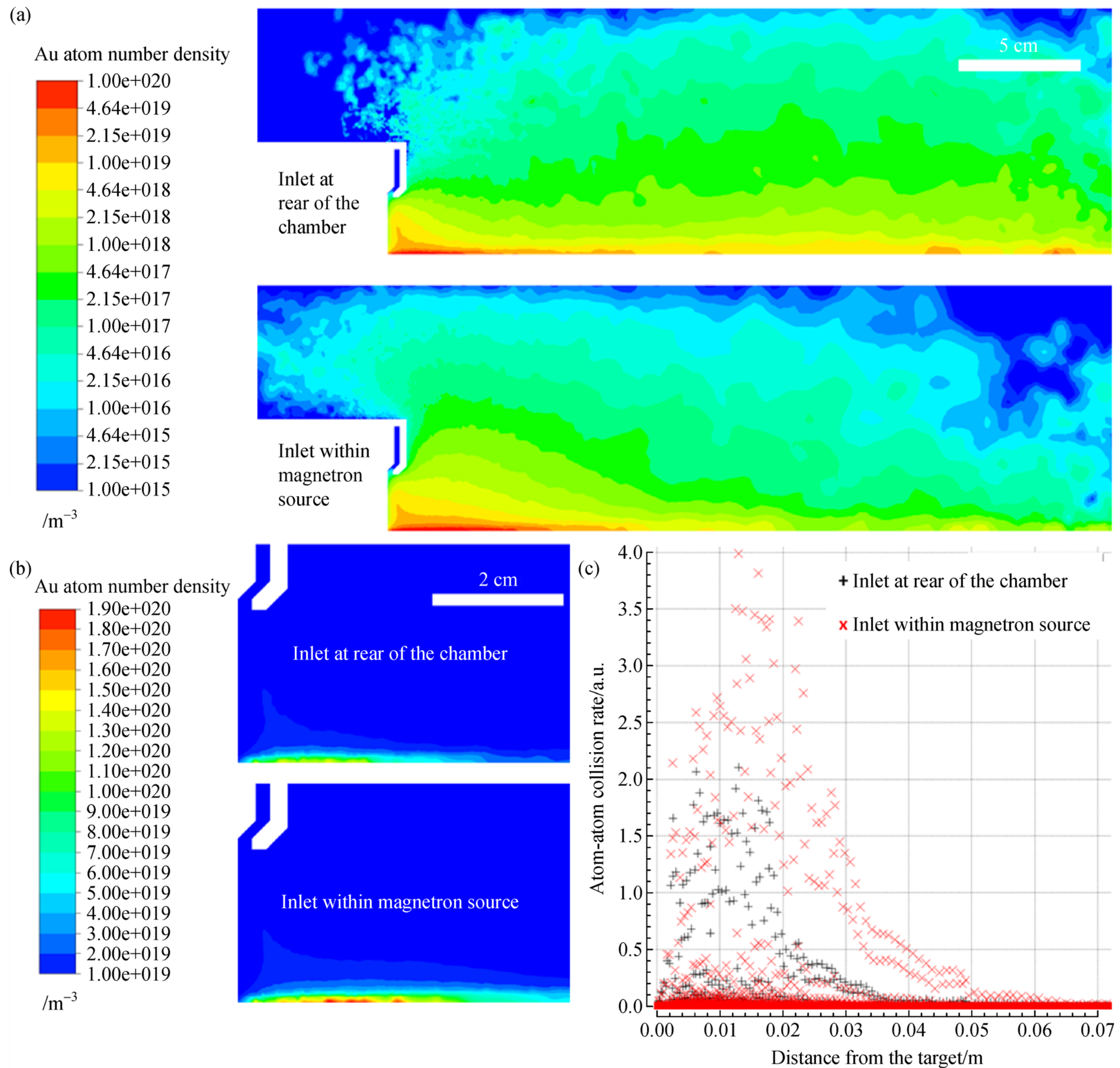

Fig. 8 (a) Au single atom number density profile inside the condensation chamber in the case where the gas is provided from the rear of the chamber (top) and from within the magnetron source (bottom). A logarithmic scale is used to show the number density distribution. (b) Au single atom number density profile in a region close to the target surface, in the case where the gas is provided from the rear of the chamber (top) and from within the magnetron source (bottom). A linear scale is used to show the number density distribution. (c) The probability of Au atom–atom collision in front of the sputtering target, if the gas inlet is within the magnetron source (red cross symbol) and at the rear of the chamber (gray dash symbol). Reprinted with permission from ref. [35], copyright 2021, AIP Publishing.

high-rate cluster production instrument, the carrier gas should be injected into the condensation chamber at a place as close to the sputtering target surface as possible to reduce redeposition of sputtered atoms onto the sputtering target and to increase atom-atom collision probability.

Four different geometries of condensation chambers have been simulated (Fig. 9): two “standard” cylindrical shapes with a cross-sectional diameter of 200 and 100 mm and two conical shapes, both with a diameter of 100 mm, one with an apex angle of 90° and the other one with an apex angle of 60°. These simulations indicated, theoretically, that the conical design with a smaller apex angle is the most efficient. By reducing the chamber diameter and reducing the apex angle for the conical chamber, the gas velocity profile was optimized in such a way that the gas velocity close to the walls was increased. As a result, the probability of attachment of clusters to the walls (and hence lost from the cluster generation process) was reduced. It was also experimentally proved that the new design performs more than 5 times better than the standard cylindrical design.

In addition, it was found that the measured cluster flux increases monotonically with the sputtering power applied and the Ar gas flow rate supplied, until the experiment was

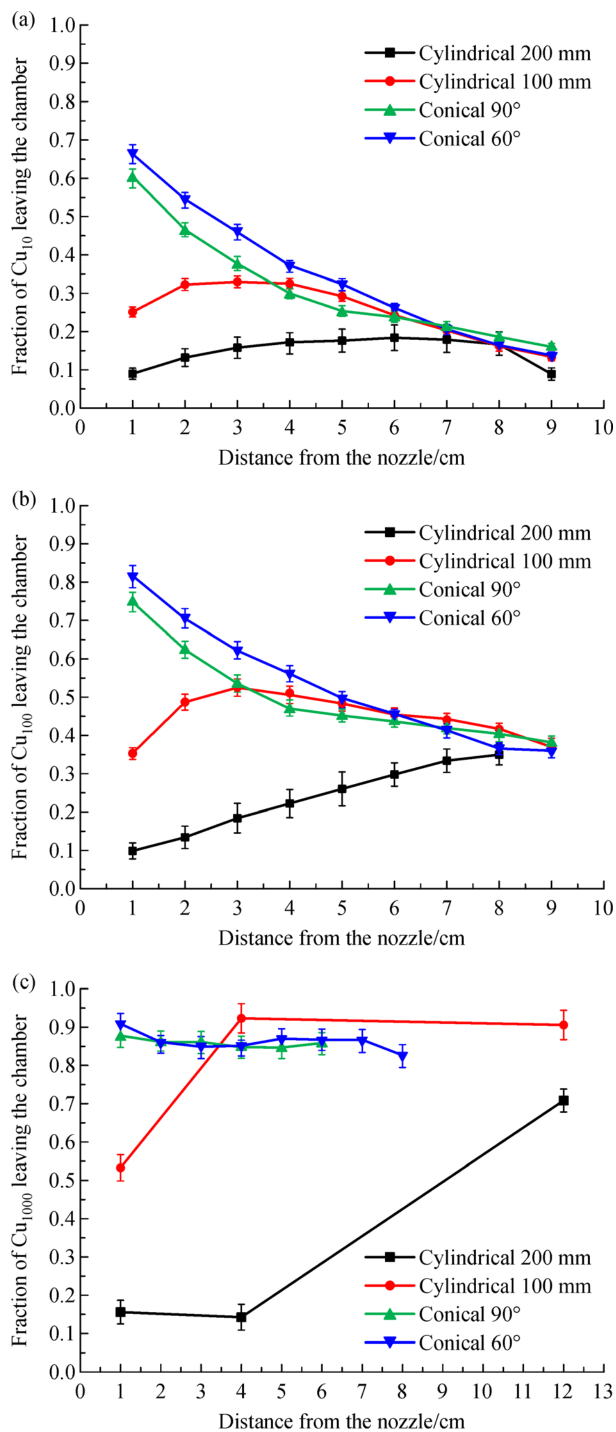

Fig. 9 Fraction of clusters departing from lines perpendicular to the chamber axis and successfully going out through the nozzle *vs.* the distance of such lines from the nozzle. The results for clusters of different sizes are shown here: (a) 10 atoms per cluster, (b) 100 atoms per cluster, and (c) 1000 atoms per cluster. Reprinted with permission from ref. [35], copyright 2021, AIP Publishing.

terminated at a sputtering power of 50 W and an Ar flow rate of 150 mL·min^{-1} [35]. Although it is almost impossible to raise the Ar flow rate further as the plasma sputtering would breakdown, there is still a scope to increase the sputtering power to 250 W. It is speculated that the cluster throughput might increase exponentially when the sputtering power is beyond 100 W, as the resulted high number density of vaporised atoms would speed up the formation of clusters. Further experiments are needed to verify this hypothesis.

3 Pulsed microplasma cluster source

A PMCS (Fig. 10) was first introduced by Milani et al. [60] and consists of a ceramic cell with two rods (the electrodes) mounted on one axis of the cell, one being anode and the other cathode. The cathode is the material that needs to be vaporized to form clusters. Perpendicularly to the electrodes, a solenoid pulsed valve provides inert gas, Ar or He, to the cavity at a pressure of ~10 bar with pulses of a few hundreds of microseconds [61] (Fig. 10(a)) and frequency of ~5 Hz. When the valve is closed, the pressure inside the PMCS is ~10^{-7} torr.

A PMCS is very similar to a PACIS [62–70]. From a technical point of view, it differs from the latter in the geometry of the nozzle, which is cylindrical only for the PMCS, and in the space surrounding the cathode and anode being much bigger, typically in the order of a few cubic centimeters [71]. Like a PACIS, the PMCS has a pulsed valve providing inert gas in a series burst of high-pressure gas pulses. In a PMCS, however, the gap between the cathode and anode does not face the pulsed gas valve, which instead eject the gas directly toward the cathode surface. When the gas pulse is in proximity of the cathode, an electrical discharge is provided, typically with a duration of ~50 μs. In this case, because of the gas confinement on the cathode surface and of a much larger volume available around the cathode, it produces a localized plasma erosion on the cathode and sputters out mainly neutral species [60,72]. Due to the non-uniformity of the gas density around the cathode, different areas of the target will have different sputtering yields [73]. To have an even target erosion in the process, the cathode is attached to a motor which makes it continuously rotating throughout the process, always providing a fresh surface for the next erosion pulse (Fig. 10(a)). The PMCS may be equipped with a system of aerodynamic lenses, which, as explained below, helps to focus the clusters into a cluster beam and to even have a control on the cluster size (Fig. 10(b)). Typically, a PMCS is installed in a sequential pumping system to provide HV or UHV in the deposition chamber (Fig. 10(c)). This provides sufficient pressure difference between the cluster source and the deposition regions, thus establishing a supersonic expansion of the cluster-gas carrier mixture giving rise to a supersonic collision-less cluster beam [74].

In a PMCS, cluster condensation occurs in a way similar to a magnetron sputtering cluster source. The atoms

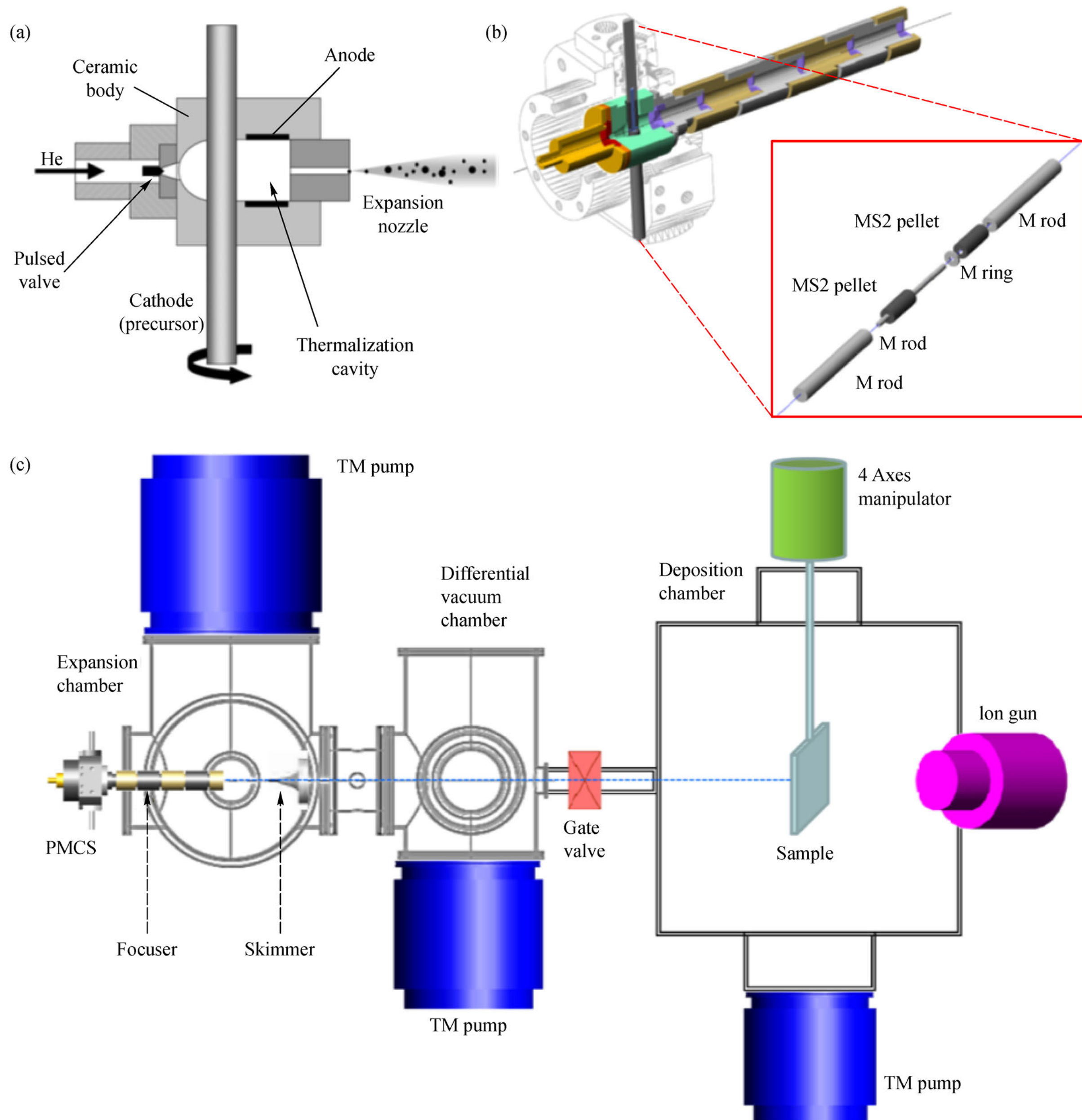

Fig. 10 (a) Cross section of a PMCS, featuring the main constituents. Reprinted with permission from ref. [71], copyright 1999, IOP Publishing. (b) 3-D sketch of a PMCS with a system of aerodynamic lenses mounted on the nozzle exit. The rod (cathode) in specifically designed for the experiment in ref. [75]. Here a MoS_2 target needed to be eroded but, because of its mechanical fragility and electrical resistivity, a system of Mo ring and holder rods hosting two MoS_2 pellet cylinders has been designed, so to overcome such problems. (c) Schematics of a PMCS (left) mounted on a typical supersonic cluster beam deposition system, showing the different sections in the sequential pumping. Reprinted with permission from ref. [75], copyright 2015, IOP Publishing.

ablated from the cathode surface after the electrical discharge thermalise in the high-pressure inert gas surrounding the cathode. Because of the nature of the process, which involves the sputtered atoms to be in a high-pressure environment, there is a small percentage of clusters produced being positively or negatively charged, respectively around 10% and 2% of the total amount. Clusters generated by a PMCS generally follow a log-normal size distribution [60].

With the aim to focus and to size-control the clusters deposited, Piseri and coworkers [76] implemented the source chamber by adding a simple device, called focuser. This element is a circular disk with eight holes drilled at the circumference edge, designed to be mounted inside the PMCS just before the nozzle. Only a small variable gap, in the range of 0.2–0.5 mm, is left between the focuser and the nozzle. With the employment of the focuser, the gas and the clusters transported are forced to go through two

sudden turns. The light particles, having a smaller inertia, easily follow the gas streamlines. The heavy particles, on the other hand, have bigger inertia and will follow paths with radii of curvature much larger than the carrier gas streamlines and thus they collide and deposit on the nozzle walls. Clusters of intermediate size, behaving somewhere in the middle of the two extreme cases stated above, focus effectively on the nozzle axis. The influence of the focuser on the cluster deposition is shown in Fig. 11, in which Fig. 11(a) shows the photographs of carbon clusters deposited using the PMCS with and without a focuser. Both depositions have been performed under the same source operating conditions. It is evident that the focuser increases the intensity of the beam at the axis. With a quartz microbalance at a distance of 300 mm from the nozzle, cluster mass flux has been measured at 1.5–2 $nm \cdot s^{-1}$ and 3–5 $nm \cdot min^{-1}$ respectively for the configuration with and without the focuser. Atomic force microscopy (AFM) measurements (Fig. 11(b)) also show a shift in cluster diameter toward smaller value by ~30% if the focuser is employed.

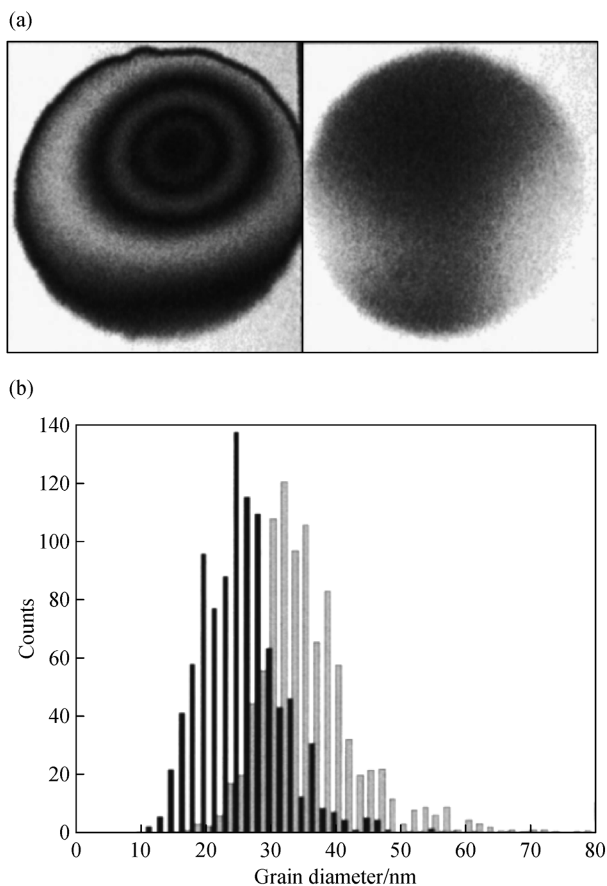

Fig. 11 (a) Photographs of a cluster film deposited at 300 mm from the source with (left) and without (right) the use of a focuser; (b) histogram of the high magnification AFM results showing the two size distributions for the focused and unfocused cluster deposition, respectively in black and gray color. Reprinted with permission from ref. [76], copyright 2001 AIP, Publishing.

The results obtained are strongly dependent on the pressure and on the gap between the focuser and the nozzle, which also affects the pressure at the nozzle [61]. In the case the pressure is lower, the cluster trajectory may in fact diverge from the nozzle axis after crossing it, while for higher pressures clusters will uniformly follow the streamlines, resulting a poor focus. It has been proven with simulations that the pressure at the entrance of the nozzle depends on the gap between the focuser and the nozzle. In particular, the smaller the gap, the lower the pressure at the entrance of the nozzle. Therefore, by tuning the gap it is possible to select the cluster size to be focused (critical size). Figure 12 shows the dependence of the critical size on the focuser-nozzle gap at different Reynolds number, i.e. at different initial gas pressure in the PMCS, prior to the focuser [77]. Decreasing the gap, which results in decreasing the pressure at the entrance of the nozzle, causes the clusters to experience less drag force from the carrier gas. Bigger particles, with higher inertia, will then diverge and the critical size decreases. Nevertheless, at higher values of Reynolds number, the carrier gas becomes “more viscous” (in real experiments it means higher initial pressure), so the critical size increases as the gas can exert the amount of drag force needed to keep bigger particles close to the streamlines. To quantify the performance of the focuser, simulations on the divergence of clusters with different size and different starting position were carried out by Vahedi Tafreshi et al. and results show that even if the Brownian motion of clusters is taken into account, it cannot suppress the focusing effect of the focuser [78] (Fig. 13).

Following the same principle, a set of aerodynamic lenses made up of several cylindrical sections with an

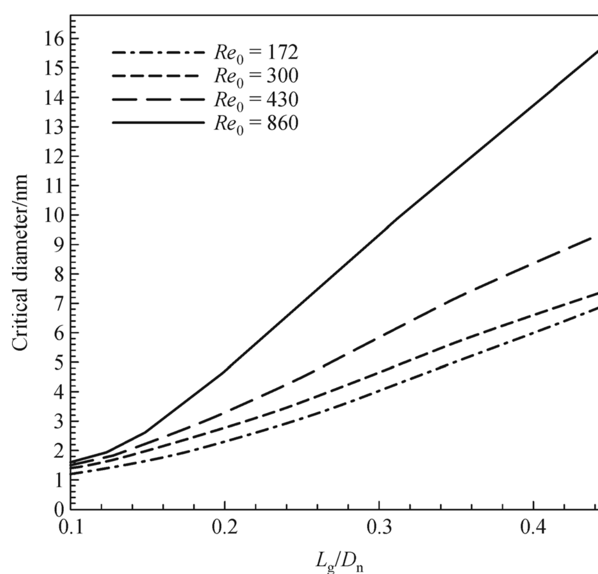

Fig. 12 Critical diameter as a function of the gap distance for different values of the Reynolds number Re_0. Reprinted with permission from ref. [61], copyright 2002, Taylor & Francis.

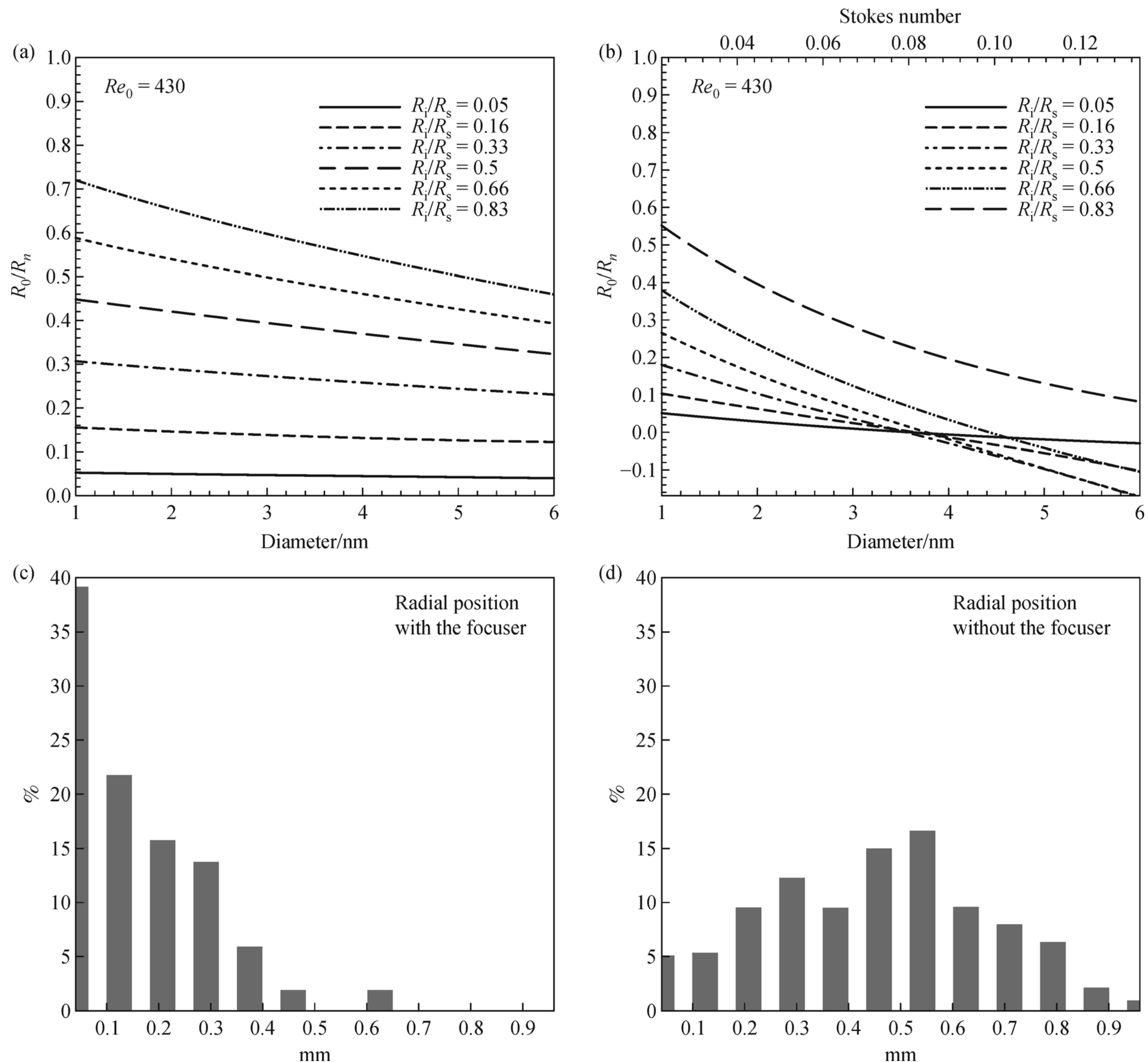

Fig. 13 (a) Radial displacement at the end of the nozzle as a function of the particle diameter for different particle injection radial position without the focuser; (b) same as in (a) but with the use of a focuser. Reprinted with permission from ref. [61], copyright 2002, Taylor & Francis. (c) Histogram of the radial displacement of the particles exiting the nozzle without the use of a focuser. Brownian motion is considered in the calculation; (d) same as in (c) but with the use of a focuser. Reprinted with permission from ref. [78], copyright 2002, Springer Nature.

opening in the axis can be mounted after the nozzle (Fig. 10(b)), with the scope of size-controlling the ejected neutral clusters and of focusing them into a cluster beam. Figure 14 shows a schematic of its working principle. Analogously of the above-mentioned focuser, by tuning the apertures of the lenses (the gap in the case of the focuser) it is possible to “select” the size of the outgoing clusters. Big particles, with a large Stokes number ($St \gg 1$), have high inertia and are more resilient at following the carrier gas streamlines. On the other hand, small particles, with a small Stokes number ($St \ll 1$), follow very precisely the gas streamlines, diverging whenever they diverge. Only the particles with the desired size, i.e., $St \approx 1$, will be focused toward the beam axis and will exit in the form of a collimated cluster beam [79–81].

Generally, a PMCS has great advantages such as high particle flux, stability and high reproducibility [72]. Also, the flux and size distribution of the produced clusters can be controlled by changing process parameters such as voltage applied to the cathode and pulse duration, the pulsed gas valve opening time or frequency, or by modifying the aerodynamic lens sequence or geometry, the nozzle diameter or even the type of gas carrier employed. It has been proven to be also versatile in the production of different cluster material, such as C, Ti, Ni, Fe, Si, W, Mo, MoS_2, WS_2, Au, Ag, Pt, Pd, Zr, and V. Due to the sputtering process being catalyzed by a DC discharge, the PMCS is less efficient in sputtering material with poor electrical conductivity such as semiconductors or insulators. Furthermore, another limitation is the low

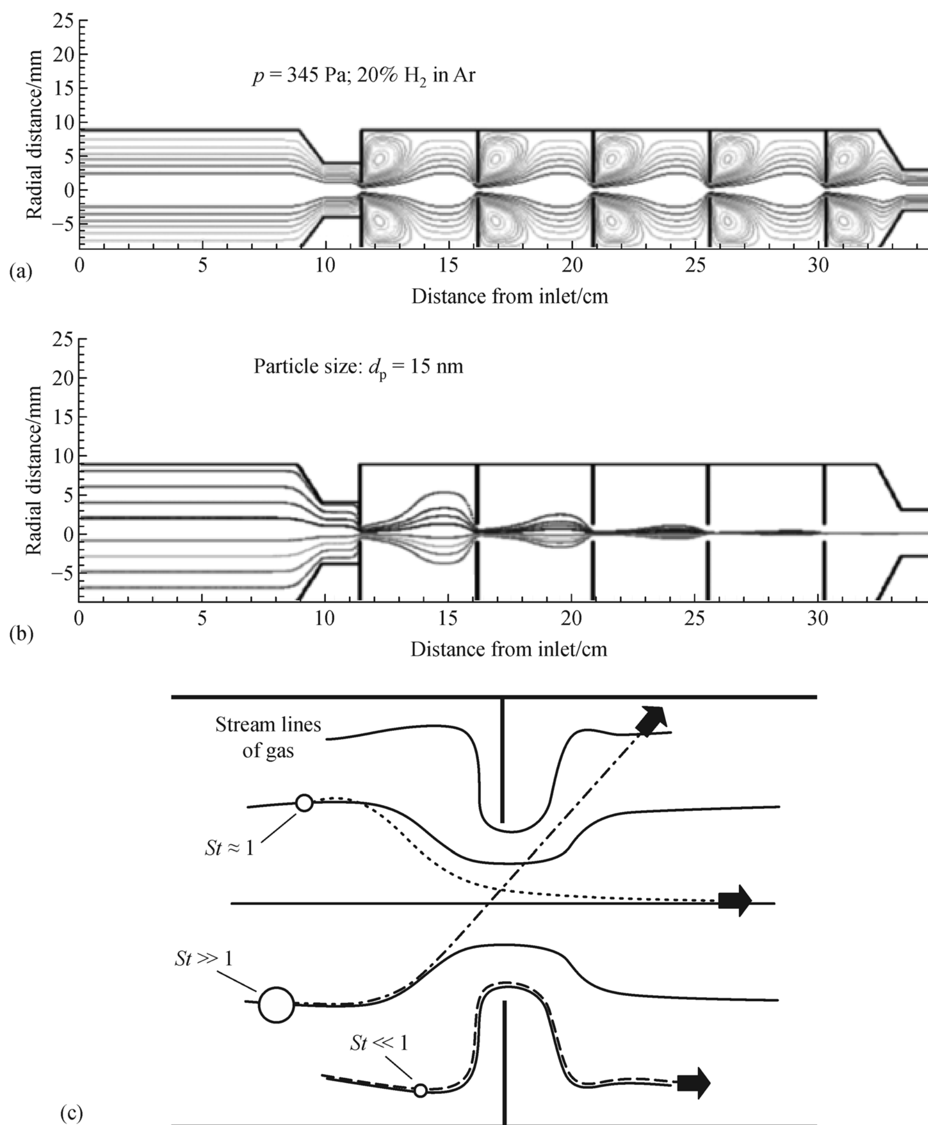

Fig. 14 (a) Gas carrier streamlines from simulation results for a pressure of 345 Pa and 20% of H_2 in Ar; (b) cluster trajectories for a particle diameter of 15 nm; (c) schematics of the cluster trajectories for different particle size, showing the principles of aerodynamic focusing and size-selection. Reprinted with permission from ref. [74], copyright 2006, IOP Publishing.

pulse frequency used to run the source, which seems unhelpful to increase the cluster flux. However, if a higher repetition rate is used, it would in fact result in the overlapping of the gas pulses, and a much more efficient pumping system would be required to retain an HV or UHV and the cluster beam supersonic expansion regime.

4 Matrix assembly cluster source

The MACS, based on a new principle of operation, was first reported in 2016 [82]. Commonly in most cluster beam deposition technologies, clusters are formed from the atomic vapor condensation with the aid of a cold bath gas, which allows the formation of dimers from three-body collision processes. However, in a MACS (schematic drawing shown in Fig. 15), clusters are formed in a cold solid argon matrix. As reported in their first attempt to scale up the cluster production with a MACS, a metal grid is cryogenically cooled using liquid helium to temperatures below 15 K (Fig. 15(a)). The grid is then exposed to an overpressure of inert gas (Ar), along with metal atom vapor, which is generated by thermal evaporation. The rare gas and the metal vapor are condensed on the grid and form a matrix, which is then eroded by an energetic Ar^+ ion beam (energy ~1 keV) generated by an ion gun. This is known as “transmission mode”, as the ion beam is applied perpendicularly to the grid surface and clusters are ejected from the opposite side of the grid (Fig. 15(b)). In this operation mode, the cluster ejection efficiency is limited by the grid transmittance, commonly ~37% [82].

To overcome this efficiency limitation, a cryogenically

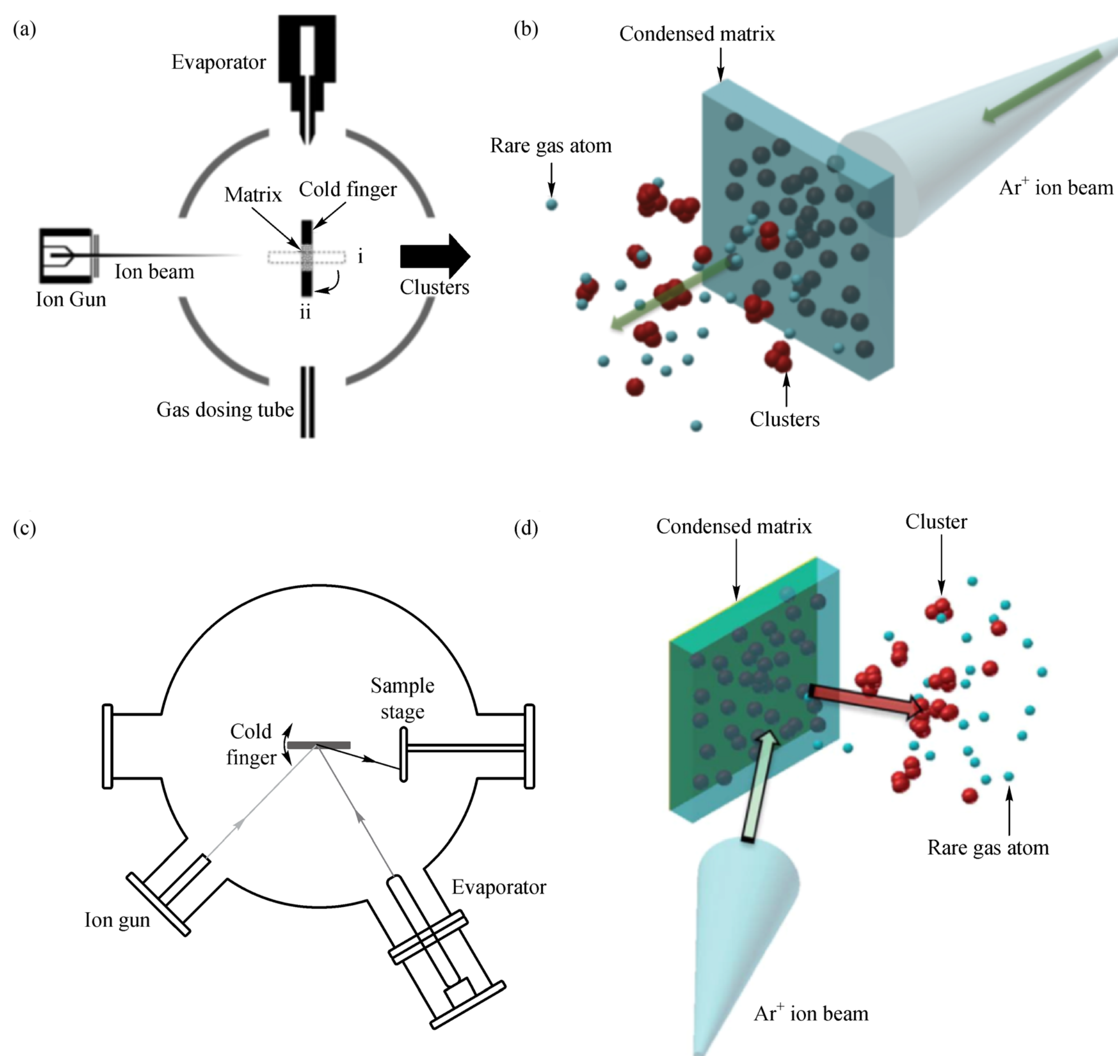

Fig. 15 (a) Schematics of a MACS in the "transmission mode"; (b) graphic representation of the Ar^+ ion beam impacting on the metal and gas condensed matrix and eroded in the "transmission mode". Reprinted with permission from ref. [82], copyright 2016, AIP Publishing. (c) Schematics of a MACS in the "reflection mode"; (d) graphic representation of the Ar^+ ion beam impacting on the metal and gas condensed matrix and eroded in the "reflection mode". Reprinted with permission from ref. [9], copyright 2016, the Royal Society of Chemistry.

cooled metal plate can be used in the place of the grid [9] (Fig. 15(c)). The inert gas and the metal vapor are condensed into a matrix on top of the metal plate. Once the matrix is formed, an Ar^+ ion beam is emitted from an ion gun and impacts the matrix from a tilted angle (Fig. 15(d)), sputtering out the formed clusters which are then deposited directly onto the substrate nearby. This is known as the "reflection mode". Both operational modes show a relatively high fraction of clusters produced per incident Ar^+ ion, of the order of ~1%. The clusters extracted in both operational modes are mainly neutral, which hinders the use of the technique if a finer cluster size selection is required. Nevertheless, the reported cluster size distributions are relatively narrow, the typical FWHM of the cluster diameter distribution being ~10% of the average diameter.

The MACS also shows a high tunability of the ejected cluster size. By increasing the relative amount of metal loading inside the condensed gas matrix, a higher mean cluster size is observed. Figure 16 shows the cluster mean size, as extrapolated from high angle annular dark field (HAADF)-STEM, depending on the metal concentration in the condensed gas matrix in the case of Au [83]. By increasing the metal content, it is possible to tune the mean cluster size from a few atoms to ~1000 atoms per cluster.

Although the process has similarities to the more widely used and better understood sputtering process, there are several factors which would differentiate the two processes, such as the bonding energy of the metal and the solid gas as well as their mutual interaction, the relative amount of the metal and the solid gas and the low temperature of the matrix [84]. A major difference between

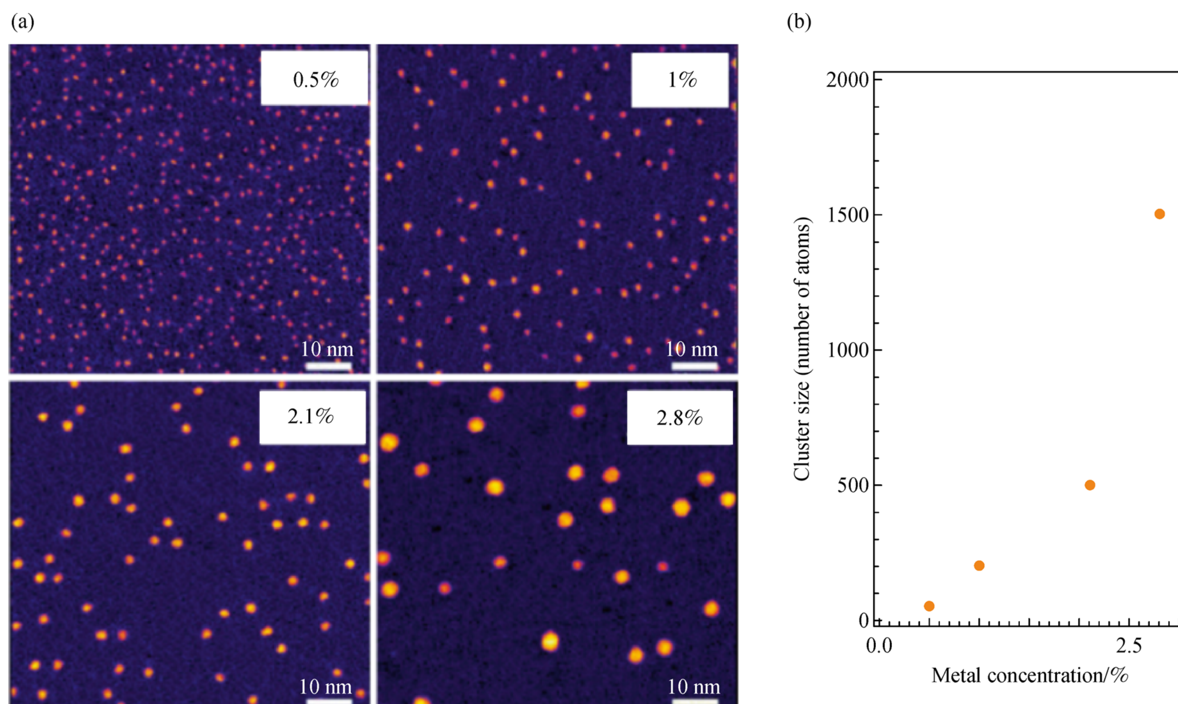

Fig. 16 (a) HAADF-STEM images for Au clusters for different concentration of Au atoms embedded in the condensed gas matrix different concentration: 0.5%, 1%, 2.1% and 2.8%. The scale bar corresponds to 10 nm; (b) plot of the cluster mean size and of the cluster beam intensity *vs.* the metal concentration in the matrix as extrapolated by the HAADF-STEM images. Reprinted with permission from ref. [83], copyright 2020, Springer.

the two processes is the presence in a MACS of another physical mechanism, the heat spike sputtering. As a consequence of the high energy exchange between the impinging Ar^+ ion (energy 1 keV) and the metal doped condensed Ar matrix (temperature 10 K), the temperature may increase up to 10000 K, far above the boiling point of Ar. These heat spikes would increase the sputtering yield by several orders of magnitude [85]. The metal-metal energy bond is, on the other hand, much higher than that of Ar-Ar or metal-Ar. For this reason, the metal atoms colliding with each other in the region of the heat spike, induced by the high-energy impacting Ar^+ ions, are likely to form a bond and stay attached, while the condensed Ar boils and evaporates.

With the help of molecular dynamics (MD) simulations, Zhao et al. proposed a model on the physical mechanism behind cluster formation and ejection using a MACS [84]. According to this model, clusters do not form during the condensation of metal vapor and inert gas on the cryogenically cooled support (either flat surface or grid, respectively for reflection or transmission mode), as the atomic kinetic energy would be too low to provide sufficient mobility for the metal atoms to collide and form a bigger particle. Instead, it is during the Ar^+ ion bombardment that the clusters form. The high energy transfer and nonlinear cascade provided by the ion impact would induce a heat spike which instantly evaporates the surface Ar atoms present in the condensed matrix as well as supplies the metal atoms with the kinetic energy necessary to increase their mobility and, therefore, to increase their probability to collide one another and form bigger particles. These metal clusters are then eroded away along with the evaporating Ar. In principle, a higher Ar^+ ion current should lead to higher mobility of the metal atoms, which means more metal-metal collisions and therefore larger particles as well as higher cluster flux (Fig. 17).

As the metal concentration in the condensed matrix increases, the metal agglomerates also become bigger as more metal atoms are involved in metal-metal collision processes. Bigger clusters are more difficult to be knocked off from the matrix, as they need a higher momentum transfer in order to be sputtered away. Nevertheless, as the metal particle is bombarded by the Ar^+ ion flux, its temperature sharply increases and the cluster melts down. During this process, it separates from the Ar matrix as it boils the Ar atoms at the interface. It then rapidly cools down to temperature below ~1000 K in approximately 1 ps, while it receives a momentum transfer from the impinging Ar^+ ions. The metal cluster is therefore pushed toward the matrix, which initially compresses and then releases the accumulated elastic potential energy to the metal cluster as it is knocked out from the condensed matrix.

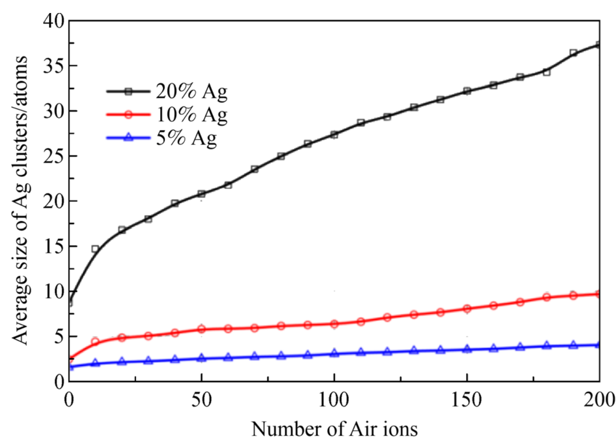

Fig. 17 MD simulation results on the average size of Ag clusters varying the number of Ar^+ ions impacting the condensed matrix for three different concentration of Ag: 5%, 10% and 20%. Reprinted with permission from ref. [84], copyright 2017, American Physical Society.

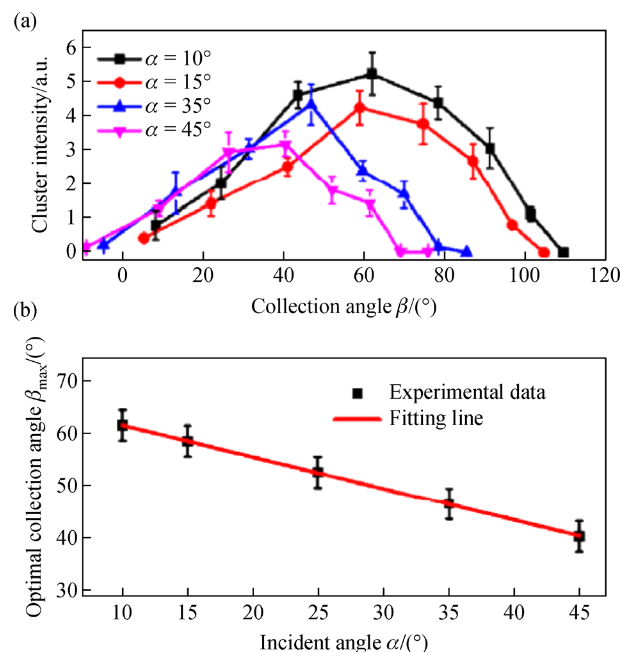

Fig. 18 (a) Experimental data of the measured cluster intensity as a function of the collection angle in the case of four different incident angle of the Ar^+ ion beam: 10°, 15°, 35° and 45° (It can be noted how a lower incident angle results in a higher overall cluster intensity, which is the integral of each curve); (b) optimal collection angle, which is the peak value of each curve in (a)), as a function of the incident angle of the Ar^+ ion beam. Reprinted with permission from ref. [86], copyright 2019, Springer.

Other parameters which should be considered, especially if a MACS is operated in "reflection mode", are the angles of Ar^+ ion incidence and of cluster collection. It has been reported [86] that decreasing the incident angle of the ion beam (more grazing incidence) would not only shift the cluster collection angle with the highest cluster yield toward the normal to the surface (which could be expected), but also increase the overall cluster flux (Fig. 18). These results have been supported by MD simulations, which show that the direct impact of Ar^+ ion on the cluster lead to an energy transfer which sublimates the Ar atoms surrounding the cluster, and then the cluster is knocked out almost normal to the surface. In the case of Ar sublimation from one side of the cluster (due to an ion impact), the cluster is ejected at a preferential tilted angle. On average, if all the possible random impacts at a fixed ion beam incident angle are considered, MD simulation results agree to a good measure to experiments.

Overall, the MACS looks very promising as a new technology to scale-up cluster deposition. Since the cluster mass flux is proportional to the Ar^+ ion beam current applied and the ion sources available on the market is capable of running with currents up to ~10 A, the cluster beam mass flux in a MACS can potentially be as high as 10 $g \cdot h^{-1}$ [9]. Cai et al. recently achieved a deposition rate of Ag clusters at 10 $mg \cdot h^{-1}$ [87] using an Ar^+ ion beam of ~1 mA. To further prove the viability of a MACS, they deposited Ag and Au clusters onto TiO_2 and Al_2O_3 powder supports, effectively preparing catalysts at the gram-scale. Two reactions have been studied: propylene combustion on Ag/TiO_2 and Ag/Al_2O_3 [87] and ozonation of nitrophenol in aqueous solution on Ag/TiO_2 and Au/TiO_2 [88]. Although results of propylene combustion are still poor compared to commercially available catalysts prepared via chemical methods, the ozonation of nitrophenol catalytic activity of Ag/TiO_2 and Au/TiO_2 is shown to be at least on the same level of traditional catalysis on the market, and no deactivation of the catalyst has been observed even after five consecutive repeated experiment with used samples.

However, the current MACS in fact works in a repeating two sequential steps, first the gas condensed matrix formation and secondly the ion bombardment-assisted cluster deposition. The reported deposition rate is measured when the matrix is bombarded by the ion beam, not taking account of the much longer time needed to form the matrix during which no cluster is emitted. Another technical issue that hinders the further scale-up of the MACS, is the contradictory requirement on temperatures from the evaporation source (the higher the better) and from the liquid helium cooled matrix (the colder the better). As these two components sit inside the same vacuum chamber, the thermal isolation has to be carefully designed to minimise the heat radiation from the evaporation source to reach the cold matrix. One solution could be to replace the evaporation source with another type of metal vapor source which does not involve high temperature processes, but at the same time provides sufficient metal atom flux. In this sense, the implementation of a magnetron sputtering device in the MACS could resolve this issue, as the magnetron sputtering is classified as cold plasma in which the sputtered ions and atoms have

a temperature close to the ambient. This would significantly reduce the thermal load in the system. The adoption of magnetron device could also potentially make the MACS to run in a continuous mode, which would pave the way for the further scaling up of the MACS technique.

5 Conclusions and outlook

Cluster beam deposition technique has the advantage of being solvent- and ligand-free, as clusters are prepared in HV or UHV. They also boast high control over cluster purity, size, and composition when compared with chemical methods. However, the low deposition rate they can currently achieve hinders the utilization of the physical methods more widely for a model catalyst study on powder substrate. Scaling up of cluster production is needed even for laboratory scale heterogenous catalysis study, and there is a much longer way to go to increase the throughput to the entry level of industrial scale.

There are many technical approaches for the cluster beam deposition technology. In this review, we selected three variation of the cluster source techniques that are the most promising for scaling up, and have given them an in-depth introduction. Briefly, the MACS has the shortest development history, but has demonstrated a convincing cluster flux of ~10 $mg \cdot h^{-1}$. Next, it needs to develop a strategy to finely control the composition of alloy clusters with the thermal evaporation device. For PMCS, the cluster generation section (the cell) has the smallest physical size among the three, which makes it very appealing to integrate multiple cells together in parallel to immediately multiply the production rate. Although bimetallic clusters could be made using alloyed cathode in a PMCS, the challenge is to find ways to improve the composition control method. Another challenge needs to be addressed is the low sputtering yield for materials with poor electrical conductivity. In the case of SGAS, it has been developed for nearly 30 years, and has demonstrated a cluster flux as high as ~20 $mg \cdot h^{-1}$ very recently. Using individually controlled multiple magnetrons (MICS), it is convenient to adjust the composition of alloy cluster by tuning the sputtering power on each sputtering target. DC, pulsed DC or RF power supply can be chosen to sputter any material that is solid at ambient temperature, which makes this technique very versatile. However, the cluster formation process, from nucleation, growth to transportation within the condensation chamber, is still not well understood, which makes it very challenging to systematically improve the cluster throughput.

Nevertheless, in the past decade, the production rate of a cluster source has been increased by a factor of 20000, from ~1 $\mu g \cdot h^{-1}$ to the level of ~20 $mg \cdot h^{-1}$, which enabled the deposition of clusters on powders for model catalyst study demonstrated by several heterogeneous catalysis reactions. To further scale up the production rate of the cluster beam technology, two possible routes have been envisaged. 1) Implementing a magnetron sputtering device in the MACS would transform it and make it possible to operate in continuous mode. Together with a more powerful ion source, it's not impossible to achieve a production rate on the level of ~10 $g \cdot h^{-1}$. 2) For the magnetron sputtering cluster source, it is estimated that a pure conical geometry for the condensation chamber could increase the cluster flux by up to 5 times when compared to the current best-performing geometry. If a HiPIMS power supply is adopted for the pure conical geometry, it might also achieve a production rate of a few gram per hour, approaching the requirements of a potential industrial application of nanoclusters, for example, as a high-performance catalyst for a niche high added-value catalysis chemical market.

Acknowledgements We thank the funding received from the European Union's Seventh Framework Programme (Grant No. FP7/2007-2013) under grant agreement No. 607417 (Catsense) and the funding from the Innovate UK under grant agreement No. 104008 (ANCOP).

Open Access This article is licensed under a Creative Commons Attribution 4.0 International License, which permits use, sharing, adaptation, distribution and reproduction in any medium or format, as long as you give appropriate credit to the original author(s) and the source, provide a link to the Creative Commons licence, and indicate if changes were made. The images or other third party material in this article are included in the article's Creative Commons licence, unless indicated otherwise in a credit line to the material. If material is not included in the article's Creative Commons licence and your intended use is not permitted by statutory regulation or exceeds the permitted use, you will need to obtain permission directly from the copyright holder. To view a copy of this licence, visit http://creativecommons.org/licenses/by/4.0/.

References

1. Haruta M, Kobayashi T, Sano H, Yamada N. Novel gold catalysts for the oxidation of carbon monoxide at a temperature far below 0 °C. Chemistry Letters, 1987, 16(2): 405–408
2. Tyo E C, Vajda S. Catalysis by clusters with precise numbers of atoms. Nature Nanotechnology, 2015, 10(7): 577–588
3. Yao C, Guo N, Xi S, Xu C Q, Liu W, Zhao X, Li J, Fang H, Su J, Chen Z, et al. Atomically-precise dopant-controlled single cluster catalysis for electrochemical nitrogen reduction. Nature Communications, 2020, 11(1): 4389
4. Jin R, Li G, Sharma S, Li Y, Du X. Toward active-site tailoring in heterogeneous catalysis by atomically precise metal nanoclusters with crystallographic structures. Chemical Reviews, 2021, 121(2): 567–648
5. Li Z, Ji S, Liu Y, Cao X, Tian S, Chen Y, Niu Z, Li Y. Well-defined materials for heterogeneous catalysis: from nanoparticles to isolated single-atom sites. Chemical Reviews, 2020, 120(2): 623–682
6. Niu Z, Li Y. Removal and utilization of capping agents in nanocatalysis. Chemistry of Materials, 2014, 26(1): 72–83
7. Du Y, Sheng H, Astruc D, Zhu M. Atomically precise noble metal nanoclusters as efficient catalysts: a bridge between structure and properties. Chemical Reviews, 2020, 120(2): 526–622
8. Rong H, Ji S, Zhang J, Wang D, Li Y. Synthetic strategies of

supported atomic clusters for heterogeneous catalysis. Nature Communications, 2020, 11(1): 5884

9. Ellis P R, Brown C M, Bishop P T, Yin J, Cooke K, Terry W D, Liu J, Yin F, Palmer R E. The cluster beam route to model catalysts and beyond. Faraday Discussions, 2016, 188(0): 39–56
10. Halder A, Curtiss L A, Fortunelli A, Vajda S. Perspective: size selected clusters for catalysis and electrochemistry. Journal of Chemical Physics, 2018, 148(11): 110901
11. Roy C, Sebok B, Scott S B, Fiordaliso E M, Sørensen J E, Bodin A, Trimarco D B, Damsgaard C D, Vesborg P C K, Hansen O, et al. Impact of nanoparticle size and lattice oxygen on water oxidation on $NiFeO_xH_y$. Nature Catalysis, 2018, 1(11): 820–829
12. Escalera-López D, Niu Y, Yin J, Cooke K, Rees N V, Palmer R E. Enhancement of the hydrogen evolution reaction from Ni-MoS_2 hybrid nanoclusters. ACS Catalysis, 2016, 6(9): 6008–6017
13. Calvo F. Nanoalloys. 2nd ed. Cambridge: Elsevier, 2020, 22
14. De Toro J A, Normile P S, Binns C. Gas-Phase Synthesis of Nanoparticles. Weinheim: Wiley-VCH, 2017, 39–55
15. Behrisch R, Eckstein W. Sputtering by Particle Bombardment. Berlin, Heidelberg: Springer Berlin Heidelberg, 2007, 33–187
16. Yamamura Y, Tawara H. Energy dependence of ion-induced sputtering yields from monatomic solids at normal incidence. Atomic Data and Nuclear Data Tables, 1996, 62(2): 149–253
17. Yamamura Y, Shindo S. An empirical formula for angular dependence of sputtering yields. Radiation Effects, 1984, 80(1–2): 57–72
18. Sigmund P. Theory of sputtering. I. Sputtering yield of amorphous and polycrystalline targets. Physical Review, 1969, 184(2): 383–416
19. Bohdansky J. A universal relation for the sputtering yield of monatomic solids at normal ion incidence. Nuclear Instruments & Methods in Physics Research. Section B, Beam Interactions with Materials and Atoms, 1984, 2(1): 587–591
20. Anders A. Deposition rates of high power impulse magnetron sputtering: physics and economics. Journal of Vacuum Science & Technology. A, Vacuum, Surfaces, and Films, 2010, 28(4): 783–790
21. Anders A. Tutorial: Reactive high power impulse magnetron sputtering (R-HiPIMS). Journal of Applied Physics, 2017, 121(17): 171101
22. Oechsner H. Sputtering—a review of some recent experimental and theoretical aspects. Applied Physics (Berlin), 1975, 8(3): 185–198
23. Penning F M. Die glimmentladung bei niedrigem druck zwischen koaxialen zylindern in einem axialen magnetfeld. Physica, 1936, 3(9): 873–894
24. Kay E. Magnetic field effects on an abnormal truncated glow discharge and their relation to sputtered thin-film growth. Journal of Applied Physics, 1963, 34(4): 760–768
25. Waits R K. Planar magnetron sputtering. Journal of Vacuum Science and Technology, 1978, 15(2): 179–187
26. Gill W D, Kay E. Efficient low pressure sputtering in a large inverted magnetron suitable for film synthesis. Review of Scientific Instruments, 1965, 36(3): 277–282
27. Lundin D, Minea T, Gudmundsson J T. High Power Impulse Magnetron Sputtering. Amsterdam: Elsevier, 2020, 1–48
28. Kashtanov P V, Smirnov B M, Hippler R. Magnetron plasma and nanotechnology. Physics Uspekhi, 2007, 50(5): 455–488
29. Martin P M. Handbook of Deposition Technologies for Films and Coatings. 3rd ed. Boston: William Andrew Publishing, 2010, 253–296
30. Huttel Y. Gas-Phase Synthesis of Nanoparticles. Weinheim: Wiley-VCH, 2017, 23–28
31. Haberland H, Karrais M, Mall M, Thurner Y. Thin films from energetic cluster impact: a feasibility study. Journal of Vacuum Science & Technology. A, Vacuum, Surfaces, and Films, 1992, 10(5): 3266–3271
32. Haberland H, Mall M, Moseler M, Qiang Y, Reiners T, Thurner Y. Filling of micron-sized contact holes with copper by energetic cluster impact. Journal of Vacuum Science & Technology. A, Vacuum, Surfaces, and Films, 1994, 12(5): 2925–2930
33. Liu C, Zhang L, Zhang S, Liu F, Wang G, Han M. Influence of discharge power on the size of the Pd cluster generated with a magnetron plasma gas aggregation cluster source. Vacuum, 2020, 179: 109486
34. Zhang C, Feng Y. Application of extended Smoluchowski equations to formation of silver nanoclusters generated by direct current magnetron sputtering source. Journal of the Physical Society of Japan, 2016, 85(9): 094606
35. Sanzone G, Yin J, Cooke K, Sun H, Lievens P. Impact of the gas dynamics on the cluster flux in a magnetron cluster-source: influence of the chamber shape and gas-inlet position. Review of Scientific Instruments, 2021, 92(3): 033901
36. Ganeva M, Peter T, Bornholdt S, Kersten H, Strunskus T, Zaporojtchenko V, Faupel F, Hippler R. Mass spectrometric investigations of nano-size cluster ions produced by high pressure magnetron sputtering. Contributions to Plasma Physics, 2012, 52(10): 881–889
37. Peter T, Polonskyi O, Gojdka B, Mohammad Ahadi A, Strunskus T, Zaporojtchenko V, Biederman H, Faupel F. Influence of reactive gas admixture on transition metal cluster nucleation in a gas aggregation cluster source. Journal of Applied Physics, 2012, 112(11): 114321
38. Polonskyi O, Solař P, Kylián O, Drábik M, Artemenko A, Kousal J, Hanuš J, Pešička J, Matolínová I, Kolíbalová E, Slavínská D, Biederman H. Nanocomposite metal/plasma polymer films prepared by means of gas aggregation cluster source. Thin Solid Films, 2012, 520(12): 4155–4162
39. González J A, Andrés J P, De Toro J A, Muñiz P, Muñoz T, Crisan O, Binns C, Riveiro J M. Co-CoO nanoparticles prepared by reactive gas-phase aggregation. Journal of Nanoparticle Research, 2008, 11(8): 2105–2111
40. Marek A, Valter J, Kadlec S, Vyskočil J. Gas aggregation nanocluster source—reactive sputter deposition of copper and titanium nanoclusters. Surface and Coatings Technology, 2011, 205: S573–S576
41. Shyjumon I, Gopinadhan M, Helm C A, Smirnov B M, Hippler R. Deposition of titanium/titanium oxide clusters produced by magnetron sputtering. Thin Solid Films, 2006, 500(1): 41–51
42. Smirnov B M, Shyjumon I, Hippler R. Formation of clusters through generation of free atoms. Physica Scripta, 2006, 73(3): 288–295
43. Román García E L, Martínez-Orellana L, Díaz Lagos M, Huttel Y. Device and method for manufacturing nanoparticles. WO Patent, 2011, WO2011089298: A1
44. Xu Y, Wang J. Magnetic properties of heterostructured Co-Au

nanoparticles direct-synthesized from gas phase. IEEE Transactions on Magnetics, 2007, 43(6): 3109–3111

45. Pearmain D, Park S J, Abdela A, Palmer R E, Li Z Y. The size-dependent morphology of Pd nanoclusters formed by gas condensation. Nanoscale, 2015, 7(46): 19647–19652
46. Krishnan G, Verheijen M A, ten Brink G H, Palasantzas G, Kooi B J. Tuning structural motifs and alloying of bulk immiscible Mo-Cu bimetallic nanoparticles by gas-phase synthesis. Nanoscale, 2013, 5(12): 5375–5383
47. Aktaş S, Thornton S C, Binns C, Lari L, Pratt A, Kröger R, Horsfield M A. Control of gas phase nanoparticle shape and its effect on MRI relaxivity. Materials Research Express, 2015, 2(3): 035002
48. Martínez L, Díaz M, Román E, Ruano M, Llamosa P D, Huttel Y. Generation of nanoparticles with adjustable size and controlled stoichiometry: recent advances. Langmuir, 2012, 28(30): 11241–11249
49. Llamosa D, Ruano M, Martínez L, Mayoral A, Roman E, García-Hernández M, Huttel Y. The ultimate step towards a tailored engineering of core@shell and core@shell@shell nanoparticles. Nanoscale, 2014, 6(22): 13483–13486
50. Ruano M, Martínez L, Huttel Y. Investigation of the working parameters of a single magnetron of a multiple ion cluster source: determination of the relative influence of the parameters on the size and density of nanoparticles. Dataset Papers in Science, 2013, 2013: 597023
51. Gudmundsson J T, Brenning N, Lundin D, Helmersson U. High power impulse magnetron sputtering discharge. Journal of Vacuum Science & Technology. A, Vacuum, Surfaces, and Films, 2012, 30(3): 030801
52. Anders A. Discharge physics of high power impulse magnetron sputtering. Surface and Coatings Technology, 2011, 205: S1–S9
53. Lundin D, Sarakinos K. An introduction to thin film processing using high-power impulse magnetron sputtering. Journal of Materials Research, 2012, 27(5): 780–792
54. Polonskyi O, Peter T, Mohammad Ahadi A, Hinz A, Strunskus T, Zaporojtchenko V, Biederman H, Faupel F. Huge increase in gas phase nanoparticle generation by pulsed direct current sputtering in a reactive gas admixture. Applied Physics Letters, 2013, 103(3): 033118
55. Zhang C, Tsunoyama H, Akatsuka H, Sekiya H, Nagase T, Nakajima A. Advanced nanocluster ion source based on high-power impulse magnetron sputtering and time-resolved measurements of nanocluster formation. Journal of Physical Chemistry A, 2013, 117(40): 10211–10217
56. Straňák V, Block S, Drache S, Hubička Z, Helm C A, Jastrabík L, Tichý M, Hippler R. Size-controlled formation of Cu nanoclusters in pulsed magnetron sputtering system. Surface and Coatings Technology, 2011, 205(8): 2755–2762
57. Pilch I, Söderström D, Brenning N, Helmersson U. Size-controlled growth of nanoparticles in a highly ionized pulsed plasma. Applied Physics Letters, 2013, 102(3): 033108
58. Pilch I, Söderström D, Hasan M I, Helmersson U, Brenning N. Fast growth of nanoparticles in a hollow cathode plasma through orbit motion limited ion collection. Applied Physics Letters, 2013, 103(19): 193108
59. Arslanbekov R R, Kudryavtsev A A, Tobin R C. On the hollow-cathode effect: conventional and modified geometry. Plasma Sources Science & Technology, 1998, 7(3): 310–322
60. Milani P, Ferretti M, Piseri P, Bottani C E, Ferrari A, Li Bassi A, Guizzetti G, Patrini M. Synthesis and characterization of cluster-assembled carbon thin films. Journal of Applied Physics, 1997, 82(11): 5793–5798
61. Tafreshi H V, Benedek G, Piseri P, Vinati S, Barborini E, Milani P. A simple nozzle configuration for the production of low divergence supersonic cluster beam by aerodynamic focusing. Aerosol Science and Technology, 2002, 36(5): 593–606
62. Ganteför G, Siekmann H R, Lutz H O, Meiwes-Broer K H. Pure metal and metal-doped rare-gas clusters grown in a pulsed ARC cluster ion source. Chemical Physics Letters, 1990, 165(4): 293–296
63. Siekmann H R, Lüder C, Faehrmann J, Lutz H O, Meiwes-Broer K H. The pulsed arc cluster ion source (PACIS). Zeitschrift für Physik D, Atoms, Molecules and Clusters, 1991, 20(1): 417–420
64. Cha C, Ganteför G, Eberhardt W. New experimental setup for photoelectron spectroscopy on cluster anions. Review of Scientific Instruments, 1992, 63(12): 5661–5666
65. Lu W, Huang R, Ding J, Yang S. Generation of fullerenes and metal-carbon clusters in a pulsed arc cluster ion source (PACIS). Journal of Chemical Physics, 1996, 104(17): 6577–6581
66. Blessing N, Burkart S, Ganteför G. Production of large metallo-carbohedrene clusters using a pulsed arc cluster ion source. The European Physical Journal D—Atomic, Molecular. Optical and Plasma Physics, 2001, 17(1): 37–41
67. Wang H, Zhang X, Ko Y J, Grubisic A, Li X, Ganteför G, Schnöckel H, Eichhorn B W, Lee M S, Jena P, et al. Aluminum Zintl anion moieties within sodium aluminum clusters. Journal of Chemical Physics, 2014, 140(5): 054301
68. Bettac A, Köller L, Rank V, Meiwes-Broer K H. Scanning tunneling spectroscopy on deposited platinum clusters. Surface Science, 1998, 402–404: 475–479
69. Klipp B, Grass M, Müller J, Stolcic D, Lutz U, Ganteför G, Schlenker T, Boneberg J, Leiderer P. Deposition of mass-selected cluster ions using a pulsed arc cluster-ion source. Applied Physics. A, Materials Science & Processing, 2001, 73(5): 547–554
70. Pietsch S, Dollinger A, Strobel C H, Park E J, Ganteför G, Seo H O, Kim Y D, Idrobo J C, Pennycook S J. The quest for inorganic fullerenes. Journal of Applied Physics, 2015, 118(13): 134302
71. Barborini E, Piseri P, Milani P. A pulsed microplasma source of high intensity supersonic carbon cluster beams. Journal of Physics. D, Applied Physics, 1999, 32(21): L105–L109
72. Schmidt-Ott A. Spark Ablation. 1st ed. Singapore: Jenny Stanford Publishing, 2020, 245–271
73. Vahedi Tafreshi H, Piseri P, Benedek G, Milani P. The role of gas dynamics in operation conditions of a pulsed microplasma cluster source for nanostructured thin films deposition. Journal of Nanoscience and Nanotechnology, 2006, 6(4): 1140–1149
74. Wegner K, Piseri P, Tafreshi H V, Milani P. Cluster beam deposition: a tool for nanoscale science and technology. Journal of Physics. D, Applied Physics, 2006, 39(22): R439–R459
75. Piazzoni C, Buttery M, Hampson M R, Roberts E W, Ducati C, Lenardi C, Cavaliere F, Piseri P, Milani P. Tribological coatings for complex mechanical elements produced by supersonic cluster beam

deposition of metal dichalcogenide nanoparticles. Journal of Physics. D, Applied Physics, 2015, 48(26): 265302

76. Piseri P, Podestà A, Barborini E, Milani P. Production and characterization of highly intense and collimated cluster beams by inertial focusing in supersonic expansions. Review of Scientific Instruments, 2001, 72(5): 2261–2267
77. Fernandez de la Mora J, Rosell-Llompart J. Aerodynamic focusing of heavy molecules in seeded supersonic jets. Journal of Chemical Physics, 1989, 91(4): 2603–2615
78. Vahedi Tafreshi H, Piseri P, Barborini E, Benedek G, Milani P. Simulation on the effect of Brownian motion on nanoparticle trajectories in a pulsed microplasma cluster source. Journal of Nanoparticle Research, 2002, 4(6): 511–524
79. Hagena O F, Obert W. Cluster formation in expanding supersonic jets: effect of pressure, temperature, nozzle size, and test gas. Journal of Chemical Physics, 1972, 56(5): 1793–1802
80. De La Mora J F, Riesco-Chueca P. Aerodynamic focusing of particles in a carrier gas. Journal of Fluid Mechanics, 1988, 195(1): 1–21
81. Di Fonzo F, Gidwani A, Fan M H, Neumann D, Iordanoglou D I, Heberlein J V R, McMurry P H, Girshick S L, Tymiak N, Gerberich W W, et al. Focused nanoparticle-beam deposition of patterned microstructures. Applied Physics Letters, 2000, 77(6): 910–912
82. Palmer R E, Cao L, Yin F. Note: proof of principle of a new type of cluster beam source with potential for scale-up. Review of Scientific Instruments, 2016, 87(4): 046103
83. Spadaro M C, Cao L, Terry W, Balog R, Yin F, Palmer R E. Size control of Au nanoparticles from the scalable and solvent-free matrix assembly cluster source. Journal of Nanoparticle Research, 2020, 22(6): 139
84. Zhao J, Cao L, Palmer R E, Nordlund K, Djurabekova F. Formation and emission mechanisms of Ag nanoclusters in the Ar matrix assembly cluster source. Physical Review Materials, 2017, 1(6): 66002
85. Ilinov A, Kuronen A, Nordlund K, Greaves G, Hinks J A, Busby P, Mellors N J, Donnelly S E. Sputtering yields exceeding 1000 by 80 keV Xe irradiation of Au nanorods. Nuclear Instruments & Methods in Physics Research. Section B, Beam Interactions with Materials and Atoms, 2014, 341: 17–21
86. Spadaro M C, Zhao J, Terry W D, Liu J, Yin F, Djurabekova F, Palmer R E. Angular dependence of nanoparticle generation in the matrix assembly cluster source. Nano Research, 2019, 12(12): 3069–3074
87. Cai R, Cao L, Griffin R, Chansai S, Hardacre C, Palmer R E. Scale-up of cluster beam deposition to the gram scale with the matrix assembly cluster source for heterogeneous catalysis (propylene combustion). AIP Advances, 2020, 10(2): 025314
88. Cai R, Martelli F, Vernieres J, Albonetti S, Dimitratos N, Tizaoui C, Palmer R E. Scale-up of cluster beam deposition to the gram scale with the matrix assembly cluster source for heterogeneous catalysis (catalytic ozonation of nitrophenol in aqueous solution). ACS Applied Materials & Interfaces, 2020, 12(22): 24877–24882